ORIGINAL ARTICLE

lajss.org
Latin American Journal of Solids and Structures

www.lajss.org

Plastic softening characteristics of strength parameters of coal and its impact on stress and deformation surrounding the borehole

Xiaoran Chen[a], Yulin Lu[a]*

[a]Hebei Technology Innovation Center for Multi-Hazard Resilience and Emergency Handling of Engineering Structures, University of Emergency Management, Sanhe 065201, China. Email: cxr88@cidp.edu.cn; yllu@cidp.edu.cn

* Corresponding author

https://doi.org/10.1590/1679-7825/e9021

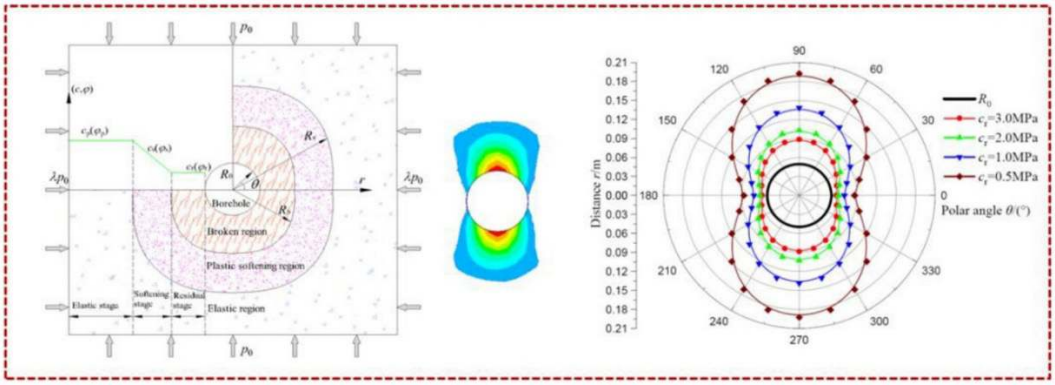
Abstract

The purpose of this study is to propose a new understanding of the influence of plastic softening of strength parameters on the mechanical properties of the coal surrounding borehole. Firstly, a thorough analysis of experimental data from previous studies reveals that the plastic softening behavior of strength parameters essentially manifests as a reduction in cohesion and a variation in internal friction angle. Subsequently, a theoretical and numerical model for deformation and stress distribution of coal surrounding borehole is established, which considers the softening effect of strength parameters and covers different regions. The maximum error between the numerical and theoretical results is found to be within 12%, which validates the reliability of the proposed analytical model. Finally, field verification results confirm that the mechanical response results derived from the model considering only the plastic softening effect of cohesion are smaller than the field-measured data, indicating that the influence of the internal friction angle must also be adequately accounted for in related analyses.

Keywords

Plastic softening; strength parameters; analytical and numerical simulation; field test

Graphical Abstract



Received February 25, 2026. In revised form August 28, 2026. Accepted October 04, 2026. Available online October 07, 2026.
https://doi.org/10.1590/1679-7825/e9021

Latin American Journal of Solids and Structures. ISSN 1679-7825. Copyright © 2026. This is an Open Access article distributed under the terms of the Creative Commons Attribution License, which permits unrestricted use, distribution, and reproduction in any medium, provided the original work is properly cited.

1 INTRODUCTION

Stress monitoring techniques, which have been widely employed to characterize the stress evolution of coal seams during excavation, play a vital role in assessing coal mining safety and preventing mine hazards. A collection of studies has shown that coal bump, coal and gas outburst, water inrush, large roof collapsing, etc. are all directly associated with the mining-induced stress (Zheng et al. 2012; Zhang et al. 2024; Geng et al. 2023). Nevertheless, the efficacy of stress monitoring is notably influenced by the deformation and damage occurring in the coal adjacent to a borehole (Zheng et al. 2012). The key to accurately acquiring stress measurement data lies in how to obtain the mechanical properties of the coal around a borehole under complex geological conditions (Zhang et al. 2026). Therefore, studying the plastic softening characteristics of strength parameters and their impact on stress and deformation is of considerable theoretical and practical significance for assessing the coal's safety and stability (Zhang et al. 2024; Geng et al.2023).

The typical stress-strain relationship of rock comprises two distinct stages, namely the pre-peak region and the post-peak region. In the post-peak region, the strength parameters often manifest softening characteristics, namely the cohesion or internal friction angle tends to decrease as the strain increases. However, the variation pattern of cohesion and internal friction angle during the plastic softening stage is a subject of debate, and to date, no unified account or accurate conclusion has been established (Jin et al. 2021). One viewpoint suggests that the essence of plastic softening lies in the reduction of cohesion, whereas the internal friction angle remains essentially unchanged (Zhang et al. 2008; González et al. 2013; Jing et al. 2018). In these analyses methods, the influence of internal friction angle on the stress and deformation was not taken into account, which results in a significant discrepancy between the calculated values and the actual data. Xu et al. (2023) argued that when coal is in the plastic zone, the development and propagation of cracks gradually reduce its cohesion to a residual value, whereas the internal friction angle remains nearly unchanged. The reduction in cohesion is the primary factor contributing to the decrease in coal strength in this region. Cui et al. (2023) pointed out that when only the softening effect of cohesion is considered, the plastic region radius of the coal around borehole is 6.663 times as large as the radius of borehole, and this result is lower than the field-measured data. It is noteworthy that the residual cohesion exhibits a reduction of 95% relative to the peak cohesion in the above-mentioned study and it must be emphasized that such a significant reduction is quite uncommon in relevant research. Since the cohesion change is directly related to the distribution of the plastic region, determining the degree of residual cohesion reduction is essential for analysis of the stress and deformation in coal.

Another viewpoint holds that two strength parameters are closely related to changes in rock strength and should exhibit a consistent variation pattern as rock strength changes. This conclusion is in stark contrast to the viewpoint of previous scholars. Li et al. (2011a) developed a nonlinear post-peak stress-strain relationship for rock, which is based on the fact that the variation trend of the internal friction angle is identical to that of cohesion when rock strength varies. Specifically, during the softening stage, the internal friction angle of rock exhibits a parabolic decrease. Yang et al. (2019) concluded from a large number of experiments that both the internal friction angle and cohesion are affected by shear damage, and proposed a damage weakening formula for the post-peak deformation of rock, which was validated by experimental data. Tong et al. (2024) presented a new practical model for the evolution of strength parameters based on standardized plastic internal variables, and demonstrated the effectiveness of simplifying the internal friction angle to a straight line in the post-peak softening stage. Fan et al. (2020) proposed a new plastic softening model based on the Mogi-Coulomb criterion, which simultaneously incorporates the weakening effects of both the internal friction angle and cohesion. Their results demonstrate that an increase in the residual internal friction angle leads to a decrease in both the plastic region radii and the surface displacement. Zhang et al. (2025) provided a simplified constitutive relationship that also accounts for the softening behavior of strength parameters by incorporating the damage states of coal surrounding borehole, namely the broken, damaged, and intact states, which correspond to the residual, plastic, and elastic deformations, respectively.

Currently, the commonly accepted view is that cohesion decreases during the plastic softening stage, but the change in internal friction angle is still a controversial issue. Although the aforementioned studies have greatly enriched research on the strength parameters of post-peak strain softening in rocks, they also have certain potential issues that merit further discussion. Firstly, most previous models examined changes in either the internal friction angle or cohesion in isolation, without simultaneously accounting for variations in both parameters. Secondly, the assumed basis for changes in strength parameters during the softening stage in early studies was not supported by subsequent field tests. Thirdly, the attribute classification of rocks is not clear, and in particular, the variation characteristics of the strength parameters of a pure coal sample have not been thoroughly analyzed. Thus, how to quantitatively characterize the softening parameters is a key component in analyzing the stress and deformation of the coal surrounding borehole. Based on previous experimental research, this study conducts an in-depth investigation into the plastic softening characteristics and general evolution law of the strength parameters of pure coal. Furthermore, an analytical model for the distribution stress and deformation of coal surrounding a borehole is theoretically established by incorporating softening parameters. Finally, the rationality of the proposed method is verified through numerical simulations and field tests.

2 Analysis of triaxial compression tests under different confining pressures

2.1 Raw data

On the basis of collecting 20 groups of coal triaxial test data reported in various literatures, the variation law of strength parameters during the plastic deformation stage is analyzed in detail in this section (Zhang et al. 2020; Yang et al. 2006; Yang et al. 2006; Tu et al. 2019; Li et al. 2011; Gao et al. 2017; Liu. 2018; Yang et al. 2023; Li et al. 2009; Wang et al. 2010; Su et al. 2006; Zhang et al. 2015; Zhu et al. 2023; Yang et al. 2023; Lu et al. 2022; Ajeet et al. 2024; Zhang et al. 2022). Given that the aforementioned data are obtained from coal samples, the main findings of this study are therefore validated as effective and reliable. The raw stress-strain curves corresponding to the 20 groups of coal tests are presented in Figure 1. As illustrated in Figure 1, the coal's strength exhibits a nearly linear increase with rising strain initially. Upon reaching the peak stress, it drops sharply, and a subsequent plateau in strength is observed as the strain continues to increase. It is worth noting that Figure 1 presents a large set of test data, and only principal stress and principal strain data are selected for data processing. Therefore, the residual and peak strength can be clearly identified and defined by the inflection point of the stress-strain curve.

2.2 Determination of strength parameters in plastic deformation stage

Neglecting the intermediate principal stress and using the Mohr-Coulomb (MC) criterion (Li et al. 2013), the relationship between principal stresses for triaxial compression test data can be described as follows:

$$\sigma_1 = \frac{1+\sin\varphi_j}{1-\sin\varphi_j}\sigma_3 + \frac{2c_j\cos\varphi_j}{1-\sin\varphi_j} \tag{1}$$

Where σ_1 and σ_3 are the maximum and minimum principal stresses, respectively; c_j and φ_j denote the cohesion and internal friction angle under different conditions; the subscript symbol "j" can be substituted with "p" and "r", where "p" and "r" are the abbreviations of "peak" and "residual", respectively.

When σ_3=0, namely the confining pressure is equal to zero, σ_1 is the uniaxial compression strength, then Eq.(1) can be expressed as:

$$\sigma_1 = \frac{2c_j\cos\varphi_j}{1-\sin\varphi_j} \tag{2}$$

Where σ_j is the uniaxial compressive strength corresponding to different states.

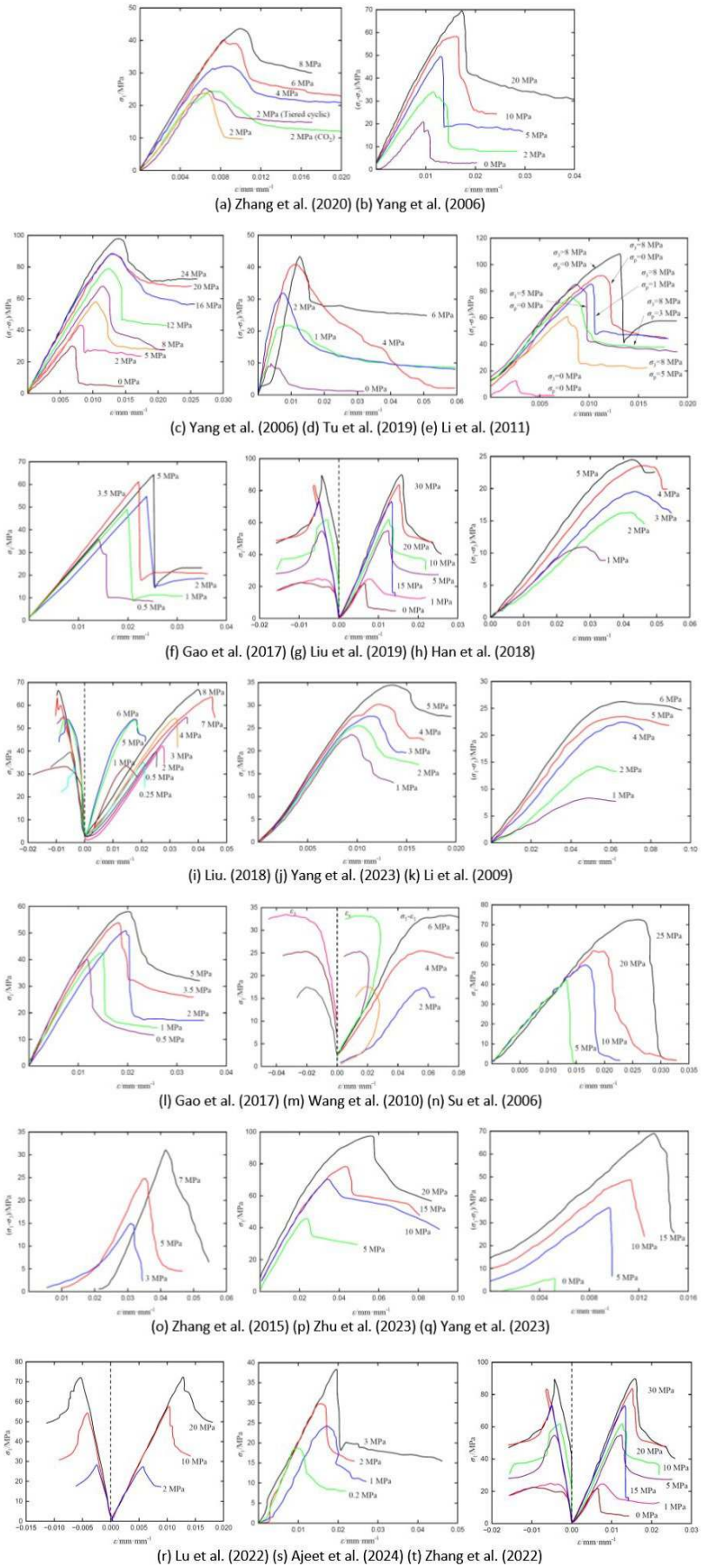
According to the induction formula (Jing et al. 2018; Tong et al. 2024), the trigonometric function can be obtained by mathematical transformation as follows:

$$\frac{1+\sin\varphi_j}{1-\sin\varphi_j} = \tan^2\left(\frac{\pi}{4}+\frac{\varphi_j}{2}\right) = \tan^2\theta_j \tag{3}$$

Where ϑ_j is the failure angle corresponding to different strength states.

Then, substituting Eq.(2) and Eq.(3) into Eq.(1), as follows,

$$\sigma_1 = \tan^2\theta_j\sigma_3 + \sigma_j \tag{4}$$



(a) Zhang et al. (2020) (b) Yang et al. (2006)

(c) Yang et al. (2006) (d) Tu et al. (2019) (e) Li et al. (2011)

(f) Gao et al. (2017) (g) Liu et al. (2019) (h) Han et al. (2018)

(i) Liu. (2018) (j) Yang et al. (2023) (k) Li et al. (2009)

(l) Gao et al. (2017) (m) Wang et al. (2010) (n) Su et al. (2006)

(o) Zhang et al. (2015) (p) Zhu et al. (2023) (q) Yang et al. (2023)

(r) Lu et al. (2022) (s) Ajeet et al. (2024) (t) Zhang et al. (2022)

Figure 1 20 groups of original complete stress-strain curves

Thus, the strength parameters can be solved using two fitting lines generated by the peak and residual strength data from the complete stress-strain curves of coal under different confining pressures. The relationship among these calculated parameters is illustrated in Figure 2. In Cartesian coordinate system, σ_3 is the horizontal axis and σ_1 is the vertical axis. As can be seen from Figure 2, σ_1 is directly proportional to σ_3. It can be readily concluded that the internal friction angles corresponding to the peak and residual strength can be directly derived from the slopes of the fitted straight lines, which are expressed as $\tan^2\vartheta_p$ and $\tan^2\vartheta_r$, respectively. Similarly, the cohesion corresponding to the peak and residual strength can be quantitatively determined on the basis of the previously derived internal friction angles and the intercepts of the fitted straight lines.

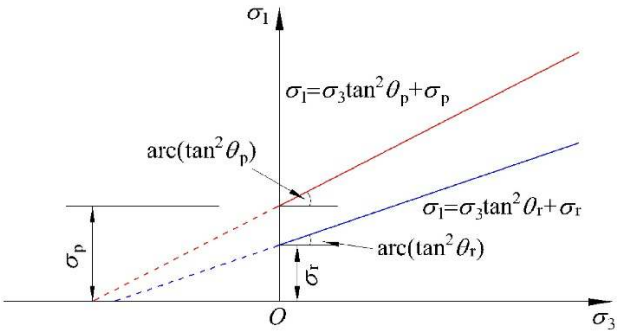


Figure 2 Solution diagram of coal peak and residual strength parameters

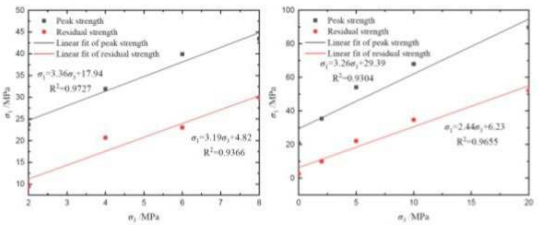
By following the aforementioned method, the peak and residual strength functions of coal can be fitted by the 20 groups of original complete stress-strain curves presented in Figure 1. The fitting results are shown in Figure 3, which clearly illustrates the relationship between the parameters.

The values of the determination coefficient R^2 are shown in Figure 4. It can be observed that these fitted functions exhibit a high degree of correlation: the determination coefficient R^2 is greater than 0.90 for the majority of coal samples, while only two groups yield results with R^2 values below 0.90, and the minimum R^2 value is 0.87. This suggests that the linear fitting function is reasonable, and it can correctly express the strength parameters of coal. Based on Eq.(4), the coal peak and residual strength parameters can be calculated, and the results can be shown in Table 1.

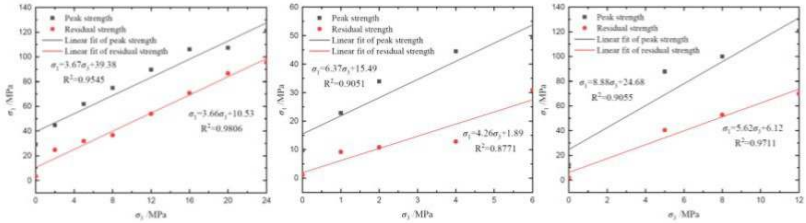
2.3 Data analysis

It can be observed from Table 1 that the residual cohesion values of the tested coal samples exhibit a significant reduction compared with the corresponding peak cohesion values, where the maximum and minimum reduction rates of cohesion reach 98.31% and 19.57%, respectively. It's important to note that the average change rate of the cohesion is 53.87%, which also implies that the cohesion plays an important part in the plastic softening stage of coal. By comparison, the maximum and minimum change rates of the internal friction angle are 87.48% and -22.94%, respectively, and the average change rate is 20.22%. On the whole, the reduction in the internal friction angle is lower than that of cohesion.

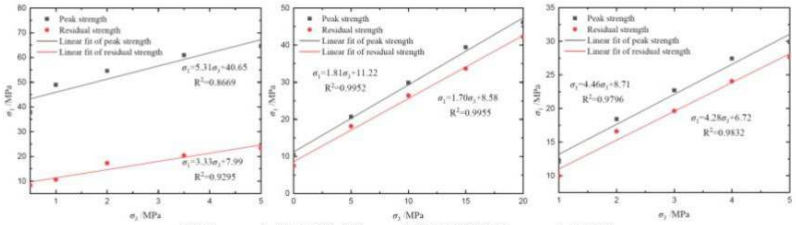
For internal friction angle, the change law is very complex. In statistical analysis, a negative change rate denotes that the residual value of the parameter is greater than its corresponding peak value, and the opposite is true for a positive change rate. Thus, in comparison with the peak internal friction angle, the residual internal friction angle shows tendencies of both decrease and increase. As shown in Figure 3(i)–(m), the results demonstrate that cases where the residual internal friction angle exceeds the peak value can also be characterized by the slopes of the fitted straight lines. When the slope of the fitting line corresponding to the residual strength is greater than that of the fitting line for the peak strength, this signifies that the residual internal friction angle is higher than its peak counterpart. It can be seen that the residual internal friction angle exceeds the peak internal friction angle in 5 groups of experimental date, which accounts for 25% of the total statistical dataset. Regarding the negative change rates of the internal friction angle, the maximum and minimum values are -22.94% and -0.38%, respectively, with an average change rate of -9.09%. This finding further demonstrates that the residual internal friction angle remains essentially unchanged across these 5 groups of experimental data. As for Figure 3(a), 3(c), and 3(h), the slopes of the two fitting lines exhibit negligible differences, and the lines are nearly parallel to one another. For the corresponding coal samples, the peak and residual strength parameters are almost equivalent. Nevertheless, across the entire statistical dataset, the average change rate of the internal friction angle is determined to be 20.22%, and 9 groups of experimental data yield change rates exceeding this average. This finding highlights that the contribution of the internal friction angle to the overall strength characteristics cannot be neglected. It is discrepant with the traditional point of view, which states that the internal friction angle remains unchanged in the plastic softening stage.



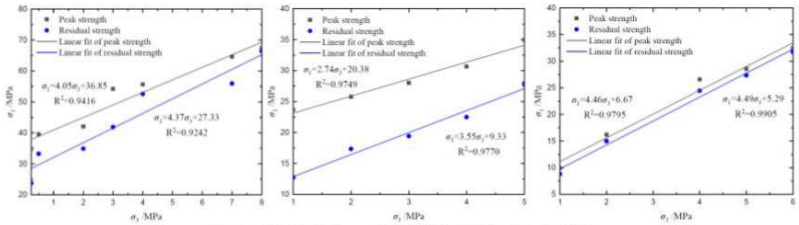
(a) Zhang et al. (2020) (b) Yang et al. (2006)



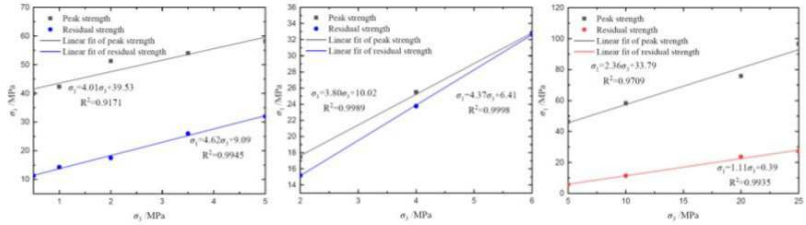
(c) Yang et al. (2006) (d) Tu et al. (2019) (e) Li et al. (2011)



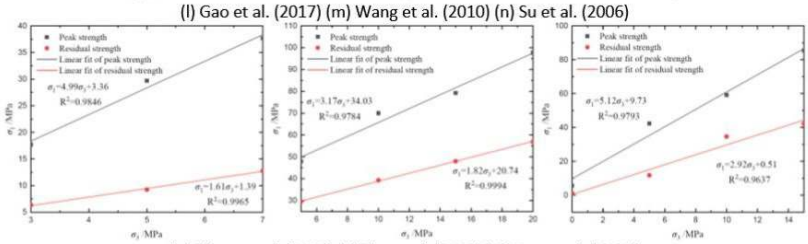
(f) Gao et al. (2017) (g) Liu et al. (2019) (h) Han et al. (2018)



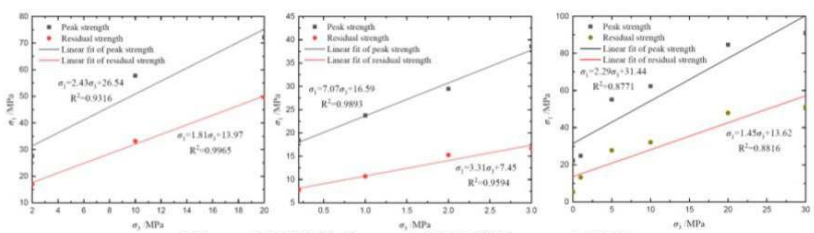
(i) Liu. (2018) (j) Yang et al. (2023) (k) Li et al. (2009)



(l) Gao et al. (2017) (m) Wang et al. (2010) (n) Su et al. (2006)



(o) Zhang et al. (2015) (p) Zhu et al. (2023) (q) Yang et al. (2023)



(r) Lu et al. (2022) (s) Ajeet et al. (2024) (t) Zhang et al. (2022)

Figure 3 Fitting results of coal strength parameters

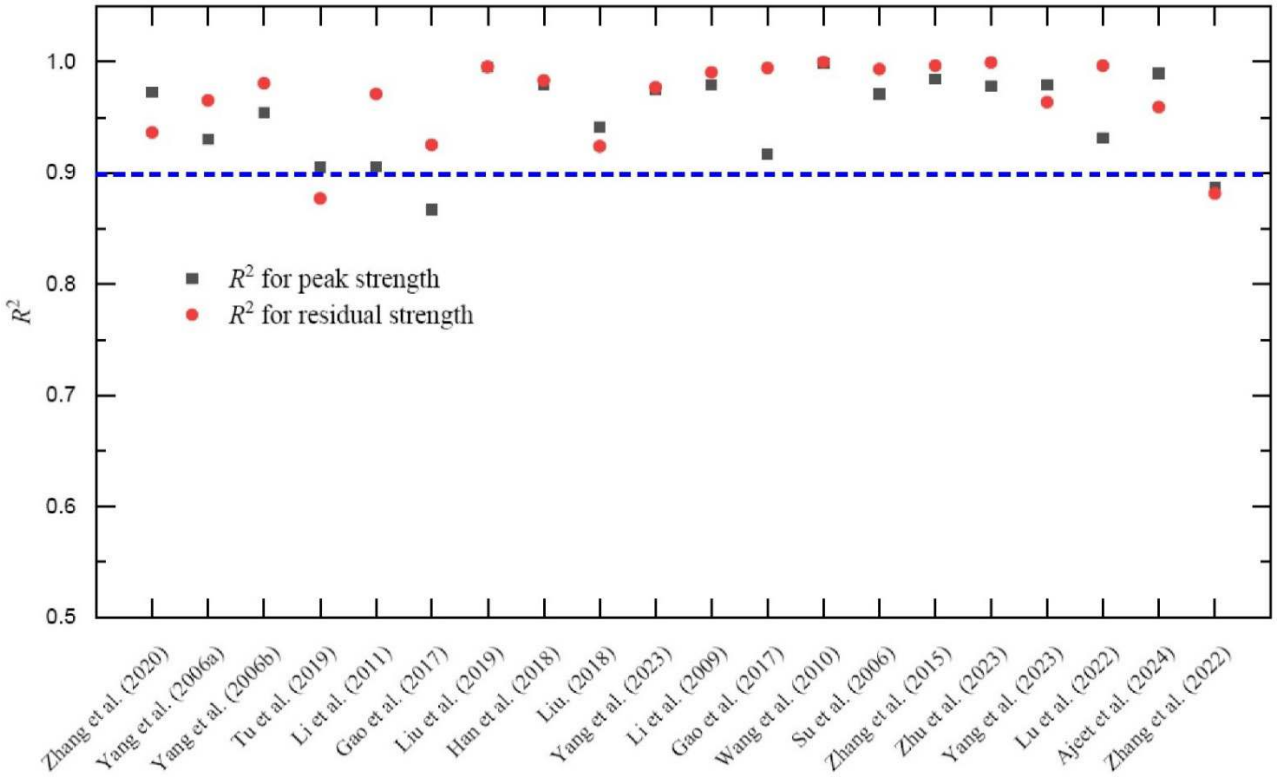


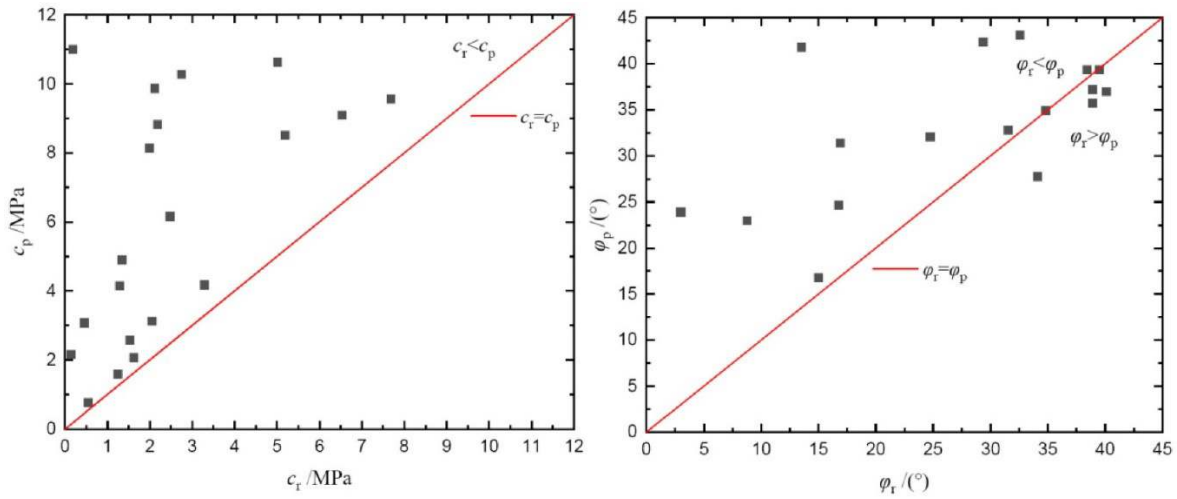
Figure 4 Determination coefficients for R^2 different strengths of coal

Table 1 Relevant parameter list of peak and residual cohesion & internal friction angle in 20 groups test data

Reference	c_p/MPa	φ_p/(°)	c_r/ MPa	φ_r/(°)	$\Delta(c_p\text{-}c_r)/\ c_p$ (%)	$\Delta(\varphi_p\ \text{-}\varphi_r)/\varphi_p$ (%)
Zhang et al. (2020)	4.89	32.79	1.35	31.53	72.43	3.84
Yang et al. (2006a)	8.14	32.06	1.99	24.76	75.50	22.76
Yang et al. (2006b)	10.28	34.89	2.75	34.82	73.22	0.18
Tu et al. (2019)	3.07	46.80	0.46	38.32	85.08	18.11
Li et al. (2011)	4.14	52.93	1.29	44.28	68.83	16.34
Gao et al. (2017)	8.82	43.10	2.19	32.57	75.18	24.44
Liu et al. (2019)	4.17	16.76	3.29	15.03	21.09	10.31
Han et al. (2018)	2.06	39.34	1.62	38.42	21.24	2.34
Liu. (2018)	9.09	37.17	6.54	38.89	28.07	-4.62
Yang et al. (2023)	6.16	27.74	2.48	34.10	59.78	-22.94
Li et al. (2009)	1.58	39.34	1.25	39.49	20.96	-0.38
Gao et al. (2017)	9.87	36.95	2.11	40.12	78.58	-8.59
Wang et al. (2010)	2.57	35.70	1.53	38.89	40.35	-8.93
Su et al. (2006)	11.00	23.89	0.19	2.99	98.32	87.48
Zhang et al. (2015)	0.75	41.79	0.55	13.52	27.17	67.64
Zhu et al. (2023)	9.56	31.37	7.69	16.91	19.57	46.09
Yang et al. (2023)	2.15	42.34	0.15	29.34	93.06	30.69
Lu et al. (2022)	8.51	24.65	5.19	16.76	39.01	32.01
Ajeet et al. (2024)	3.12	48.80	2.05	32.43	34.37	33.56
Zhang et al. (2022)	10.39	23.09	5.66	10.59	45.52	54.14
Average	6.02	35.57	2.52	28.69	53.87	20.22

In the plastic softening stage of the stress-strain curve, a number of scholars argue that the internal friction angle attenuation is so small that it can be disregarded. Nevertheless, in comparison with the findings of this study, the aforementioned research exhibits certain notable limitations. Firstly, unclear categories of rock are the major deficiency. For instance, the experimental data were sourced from a variety of rock types, including granite, marble, sandstone, coal, siltstone, and mudstone, among others; thus, the test results lack comparability (Jing et al. 2018; Cui et al.2023; Yang et al. 2019). This is primarily because the mineralogical composition and structure of different rocks vary significantly, leading to notable differences in their mechanical properties. Such differences directly influence the variation characteristics of the internal friction angle. Secondly, the small size of statistical samples constitutes another notable deficiency in these previous studies. Due to the small sample size, the results fail to comprehensively characterize the evolution law of strength parameters during the softening stage, which may compromise the reliability of the conclusions. Thirdly, the inconsistency of experimental conditions is another important factor affecting the analysis conclusions. To address these shortcomings, coal was selected as the sole research object in the present study. Specifically, a total of 20 sets of original data were collected from various publicly indexed literatures for systematic analysis, aiming to investigate the intrinsic characteristics of the plastic softening stage. All the coal samples are cylindrical standard size, i.e. 50mm in diameter and 100mm in height. The characteristics of the peak and residual strength parameters derived from the collected data are analyzed by using the MC criterion, which is depicted in Figure 5.

For the internal friction angle, the statistical results indicate that the residual values of coal in 9 groups exhibit a significant change when compared with the peak values. In total, the rate of change of 7 groups exceeds 30%, with the maximum rate of change reaching 87.48%, as shown in Table 1. Sudden cliff-like stress drop after the peak point and unobvious stress yield platform in the stress-strain curves are the prominent characteristics corresponding to the larger internal friction angle change rate, as depicted in Figure 1(n) to Figure 1(t). It should be noted that the elastic-brittle property of coal is essentially consistent with this characteristic of the stress-strain curve. Therefore, it is not feasible to directly classify the residual internal friction angle as either applicable or negligible. Instead, the triaxial test data should be the core basis for determining its practical importance.



(a) Result of cohesion (b) Result of international friction angle

Figure 5 Peak and residual strength parameters of coal samples

3 Plastic strain-softening model

The characteristic of the traditional elastic-perfectly plastic constitutive model is that the strain remains constant in the post-peak stress stage, while the key feature of plastic softening is that the strength of coal decreases significantly with increasing deformation in the post-peak stress stage, until the strength decays to the residual value. According to the previous research results (Zhang et al. 2025), there is a distinct corresponding relationship between the "3-line representation" constitutive model and the strength parameters of coal, as depicted in Figure 6. The coal's actual stress-strain curve is represented by the blue line, whereas the red line and green line denote the simplified stress-strain relationship and the softening curve of strength parameters, respectively. To facilitate calculation, the simplified stress-strain curve is typically employed in analytical methods. In this approach, coal undergoes plastic softening upon reaching the strength limit, with its deformation constrained by both elastic and fractured deformation.

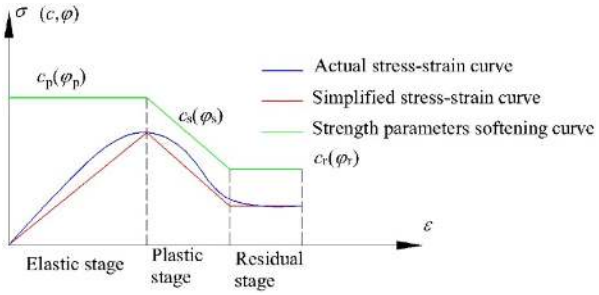


Figure 6 3 stage strain softening model

In Figure 6, it is evident that the simplified constitutive curve consists of three stages, namely the elastic stage, plastic stage, and residual stage. Strength parameters are assigned to each stage: specifically, those for the elastic stage are the peak cohesion and peak internal friction angle, while those for the residual stage are the residual cohesion and residual internal friction angle. It is a classical method to take the strength parameters as functions of strain, and this theory has been verified by many scholars (Brown et al. 1983 and Joseph. 2020). Thus, the strength parameters of coal corresponding to the stress-strain curve can be expressed as follows:

$$\begin{cases} x = x_{\mathrm{p}},\ \gamma^{\mathrm{p}} = 0 \\ x = x_{\mathrm{s}},\ 0 < \gamma^{\mathrm{p}} < \gamma^{\mathrm{p}*} \\ x = x_{\mathrm{r}},\ \gamma^{\mathrm{p}} \geq \gamma^{\mathrm{p}*} \end{cases} \tag{5}$$

Where, x denotes the strength parameters, namely cohesion c and internal friction angle φ; the subscript "p", "s" and "r" are the abbreviations of "peak", "softening", and "residual", respectively; γ^{p} is the equivalent plastic shear strain; $\gamma^{\mathrm{p}*}$ is the equivalent plastic shear strain at the beginning of residual stage, 0.01. In Eq.(5), the strength parameters during plastic softening stage can be given as:

$$x_{\mathrm{s}} = x_{\mathrm{p}} - \frac{x_{\mathrm{p}} - x_{\mathrm{r}}}{\gamma^{\mathrm{p}*}} \gamma^{\mathrm{p}} \tag{6}$$

It is possible to express the equivalent plastic shear strain using the plastic principal strain in the calculation process, and the specific expression is as follows:

$$\gamma^{\mathrm{p}} = \sqrt{\frac{2}{3}\left[\left(\varepsilon_1^{\mathrm{p}}\right)^2 + \left(\varepsilon_2^{\mathrm{p}}\right)^2 + \left(\varepsilon_3^{\mathrm{p}}\right)^2\right]} \tag{7}$$

Where, $\varepsilon^{\mathrm{p}}_i$ i=1,2,3 are the principal plastic strains, respectively.

4 Strength criterion and dilatancy coefficient

4.1 Drucker-Prager (DP) strength criterion

The selection of a strength criterion is crucial for analyzing the stress distribution of coal; otherwise, substantial errors will be incurred. Mohr-Coulomb (MC) criterion and Hoek-Brown (HB) criterion are widely adopted by scholars to investigate the mechanical properties of rock, but the major limitation of above two strength criteria is that the effect of intermediate principal stress on the yield and failure of rock is ignored, which is inconsistent with the actual situation (Zheng et al. 2012). The DP criterion is a linear representation of the generalized Mises criterion, and its key advantage is that it incorporates the influence of intermediate principal stress, thereby enabling a more accurate characterization of the actual spatial stress and deformation fields. Thus, DP criterion is selected as the analytical basis for the present study. In the plane strain analysis, the yield function of the DP criterion can be given as:

$$f = \sqrt{J_2} - \alpha_i I_1 - K_i \tag{8}$$

Where I_1 is the first stress invariant, J_2 is the second invariant of deviator stress. σ_1, σ_2, and σ_3 are the maximum, intermediate, and minimum principal stresses, respectively. Thus, I_1 and J_2 can be expressed as:

$$\begin{cases} I_1 = \sigma_1 + \sigma_2 + \sigma_3 \\ J_2 = \dfrac{1}{6}\left[(\sigma_1 - \sigma_2)^2 + (\sigma_1 - \sigma_3)^2 + (\sigma_2 - \sigma_3)^2 \right] \end{cases} \tag{9}$$

α_i and K_i, which represent material parameters related to the cohesion c_i and internal friction angle φ_i. These parameters under plane strain conditions can be described as:

$$\begin{cases} \alpha_i = \dfrac{\sin\varphi_i}{\sqrt{9 + 3\sin^2\varphi_i}} \\ K_i = \dfrac{\sqrt{3} c_i \cos\varphi_i}{\sqrt{3 + \sin^2\varphi_i}} \end{cases} \tag{10}$$

In calculations, the relationship between the principal stresses can be characterized using the intermediate principal stress coefficient m, namely

$$m = \frac{\sigma_2 - \sigma_3}{\sigma_1 - \sigma_3} \tag{11}$$

Under the assumed principal stress sequence, $0 \le m \le 1$.

Based on Eq.(8) and Eq.(11), the DP strength criterion (Pan et al. 2018) can be reformulated as:

$$f = \sigma_1 - A_i \sigma_3 - B_i \tag{12}$$

Where $\xi = \sqrt{\dfrac{m^2 - m + 1}{3}}$, $A_i = \dfrac{\xi + 2\alpha_i - m\alpha_i}{\xi - m\alpha_i - \alpha_i}$, $B_i = \dfrac{K_i}{\xi - m\alpha_i - \alpha_i}$

Generally, in accordance with the conventions of rock mechanics analysis, compressive stress is defined as positive and tensile stress as negative, then the correspondence between principal stress and stress in polar coordinates can be expressed as:

$$\begin{cases} \sigma_1 = \sigma_\theta \\ \sigma_2 = \sigma_z \\ \sigma_3 = \sigma_r \end{cases} \tag{13}$$

Where σ_θ, σ_r, and σ_z are the tangential, radial, and axial stress in polar coordinates, respectively. Hence, the general form for DP strength criterion can be also given as:

$$f = \sigma_\theta^i - A_i \sigma_r^i - B_i \tag{14}$$

In Eq.(14), the subscript and superscript symbol "*i*" can be substituted with "e", "s" and "b". Here, "e", "s" and "b" stand for the abbreviations of "elastic region", "plastic softening region", and "broken region", respectively.

4.2 Dilatancy coefficient

Dilatancy in rock mechanics refers to the phenomenon that volume strain undergoes a transition from compression to expansion prior to failure. The uniaxial compression test demonstrates that the dilatancy mainly occurs in the stress post-peak region, namely the volume deformation of coal in the elastic region can be ignored and only the deformation in the plastic softening region and broken region is considered. Generally, the coal's deformation after drilling disturbance is nonlinear, which meets the non-associated flow rule and can be determined by the plastic potential function (Zheng et al. 2012). In accordance with the material plastic potential theory, the relationship between plastic potential function and incremental principal plastic strain is formulated as:

$$\mathrm{d}\varepsilon_{ij}^{\mathrm{p}} = \mathrm{d}\lambda \frac{\partial Q}{\partial \sigma_{ij}} \tag{15}$$

Where $\mathrm{d}\varepsilon_{ij}^{\mathrm{p}}$, σ_{ij}, Q and $\mathrm{d}\lambda$ are the plastic strain increment, stress increment, plastic potential function, and plastic factor increment, respectively. This present study assumes that the plastic potential function is Q, and its form is consistent with the yield function f. Specifically, Q uses the dilatancy angle ψ instead of the internal friction angle φ. The general form of the plastic potential function Q can be written as:

$$Q = \sigma_\theta - A_i^* \sigma_r - B_i^* \tag{16}$$

Where A_i^* and B_i^* are the computed coefficients which used the dilatancy angle ψ in the plastic softening and broken stage, respectively. The subscript symbol "i" can be substituted with "s" and "b".

In elastic-plastic theory, the plastic strain increment is determined by the plastic potential function. Hence, the solution to the plastic strain increment is obtained by substituting Eq. (16) into Eq. (15), and is given as follows:

$$\begin{cases} \mathrm{d}\varepsilon_r^{\mathrm{p}} = \mathrm{d}\lambda \dfrac{\partial Q}{\partial \sigma_r} = -A_i^* \mathrm{d}\lambda \\ \mathrm{d}\varepsilon_\theta^{\mathrm{p}} = \mathrm{d}\lambda \dfrac{\partial Q}{\partial \sigma_\theta} = \mathrm{d}\lambda \end{cases} \tag{17}$$

Subsequently, by applying the non-associated flow rule, the relationship between the dilatancy coefficient and the plastic strain increment can be obtained (Zhang et al. 2025), and can be written as:

$$\Delta\varepsilon_r^{\mathrm{p}} + \chi_i \Delta\varepsilon_\theta^{\mathrm{p}} = 0 \tag{18}$$

Where χ_i is the dilatancy coefficient in different deformation stage.

By combining Eq.(17) and Eq.(18), the dilatancy coefficient in the plastic softening and broken stage can be obtained as:

$$\chi_i = A_i^* \tag{19}$$

It's important to note that when $\psi=\varphi$, the non-associated flow rule will transition to the associated flow rule. $\psi=0$, it means that no dilatancy. In this section, the dilatancy angle can be taken as $\psi=\varphi/2$.

5 Stress and deformation of coal surrounding borehole

According to the elastic-plastic theory in rock material, the deformation of coal surrounding the borehole after construction can be divided into three regions, i.e., broken region, plastic softening region, and elastic region (Li et al. 2015; He et al.2022; Anuj et al. 2023; Simanjuntak et al. 2014). The strength parameters of each region for the non-uniform stress field condition are shown in Figure 7. Some parameters can be defined as follows, p_0 and λp_0 are the vertical and horizontal stress, respectively, the lateral pressure coefficient λ is expressible as the

horizontal to vertical stress ratio. When the lateral pressure coefficient λ=1.0, the deformation zone is circular, corresponding to the uniform stress state. R_0, R_b, and R_s are the radii of the borehole, broken, and plastic softening regions, respectively. ϑ is the polar angle in polar coordinate system. When λ=1.0, the calculated model will degenerate into a uniform stress field condition.

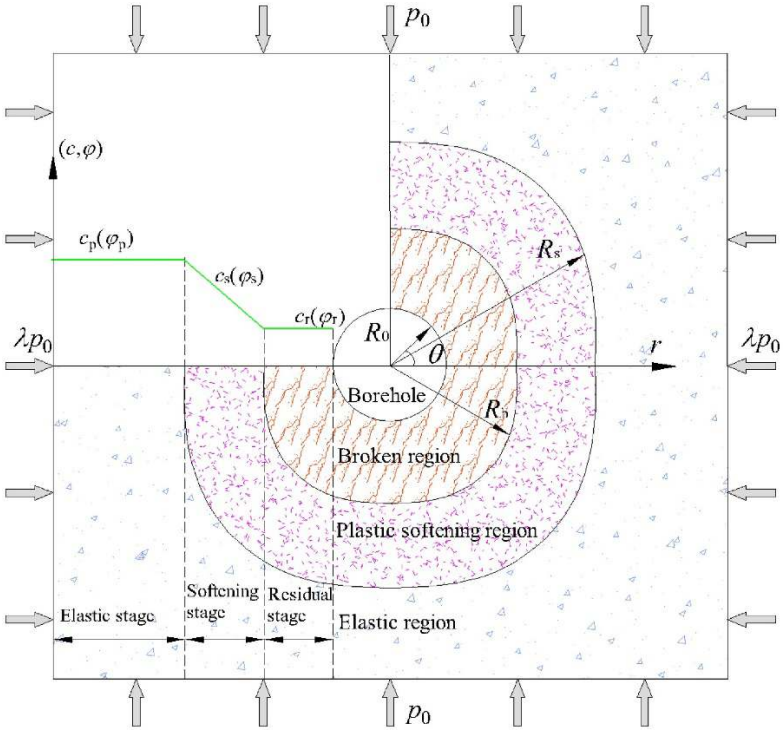


Figure 7 Coal mechanics model

5.1 Basic theory and equations

A polar coordinate system is established with the borehole center as the origin, as shown in Figure 7. Then, a continuous, homogeneous, and isotropic plane strain model is adopted to analyses the stress and deformation distribution of the coal around borehole. The effect of body force on the local stress field is insignificant and can be ignored. Accordingly, the equilibrium differential equation under different deformation regions can be expressed as (Zheng et al. 2012):

$$\frac{\mathrm{d}\sigma_{ri}}{\mathrm{d}r}+\frac{\sigma_{ri}-\sigma_{\theta i}}{r}=0 \tag{20}$$

Where σ_{ri} and $\sigma_{\vartheta i}$ are the radial and tangential stresses in different deformation regions.

For each deformation region, the satisfied geometric equation can be written as:

$$\begin{cases}\varepsilon_{ri}=\dfrac{\mathrm{d}u_i}{\mathrm{d}r}\\ \varepsilon_{\theta i}=\dfrac{u_i}{r}\end{cases} \tag{21}$$

Where ε_{ri} and $\varepsilon_{\vartheta i}$ are the radial and tangential strains in different deformation regions, respectively. u_i is the displacement in different deformation regions.

Thus, the constitutive equation can be expressed as:

$$\begin{cases} \varepsilon_{ri}=\dfrac{1-\upsilon^2}{E}\left(\sigma_{ri}-\dfrac{\upsilon}{1-\upsilon}\sigma_{\theta i}\right) \\ \varepsilon_{\theta i}=\dfrac{1-\upsilon^2}{E}\left(\sigma_{\theta i}-\dfrac{\upsilon}{1-\upsilon}\sigma_{ri}\right) \end{cases} \tag{22}$$

Where υ and E are Poisson's ratio and elastic modulus of coal, respectively.

5.2 Stress and deformation of elastic region

For deep coal masses, the deformation is mainly caused by the stress increment after borehole excavation, while the initial stress exerts no influence on additional deformation. According to previous studies (Zhang et al. 2025; Zheng et al. 2012), for the non-uniform stress field, the stress increment due to borehole excavation can be expressed as:

$$\begin{cases} \sigma_r^{\mathrm{e}}=-\dfrac{(1+\lambda)p_0}{2}\dfrac{R_{\mathrm{s}}^2}{r^2}+\sigma_r^{R_{\mathrm{s}}}\dfrac{R_{\mathrm{s}}^2}{r^2}-\dfrac{(1-\lambda)p_0}{2}\left(3\dfrac{R_{\mathrm{s}}^4}{r^4}-4\dfrac{R_{\mathrm{s}}^2}{r^2}\right)\cos 2\theta \\ \sigma_\theta^{\mathrm{e}}=\dfrac{(1+\lambda)p_0}{2}\dfrac{R_{\mathrm{s}}^2}{r^2}-\sigma_r^{R_{\mathrm{s}}}\dfrac{R_{\mathrm{s}}^2}{r^2}+\dfrac{(1-\lambda)p_0}{2}\left(3\dfrac{R_{\mathrm{s}}^4}{r^4}\right)\cos 2\theta \end{cases} \tag{23}$$

σ_r^{Rs} represents the radial stress at the elastic-plastic region interface. According to DP strength criterion Eq.(14), σ_r^{Rs} can be calculated by

$$\sigma_r^{R_{\mathrm{s}}}=\frac{(1+\lambda)p_0+2(1-\lambda)p_0\cos 2\theta-B_{\mathrm{e}}}{A_{\mathrm{e}}} \tag{24}$$

By introducing Eq.(24) into Eq.(23) and applying the geometric equation Eq.(21), the displacement and elastic strain of coal can be calculated, specifically as:

$$\begin{cases} u_{\mathrm{e}}=\dfrac{1+\upsilon}{E}r\left[\dfrac{(1+\lambda)}{2}p_0\dfrac{R_{\mathrm{s}}^2}{r^2}-\sigma_r^{R_{\mathrm{s}}}\dfrac{R_{\mathrm{s}}^2}{r^2}+\dfrac{(1-\lambda)}{2}p_0\left(3\dfrac{R_{\mathrm{s}}^4}{r^4}-4\upsilon\dfrac{R_{\mathrm{s}}^2}{r^2}\right)\cos 2\theta\right] \\ \varepsilon_r^{\mathrm{e}}=\dfrac{1+\upsilon}{E}\left[-\dfrac{(1+\lambda)}{2}p_0\dfrac{R_{\mathrm{s}}^2}{r^2}+\sigma_r^{R_{\mathrm{s}}}\dfrac{R_{\mathrm{s}}^2}{r^2}-\dfrac{(1-\lambda)}{2}p_0\left(3\dfrac{R_{\mathrm{s}}^4}{r^4}-4\dfrac{R_{\mathrm{s}}^2}{r^2}+4\upsilon\dfrac{R_{\mathrm{s}}^2}{r^2}\right)\cos 2\theta\right] \\ \varepsilon_\theta^{\mathrm{e}}=\dfrac{1+\upsilon}{E}\left[\dfrac{(1+\lambda)}{2}p_0\dfrac{R_{\mathrm{s}}^2}{r^2}-\sigma_r^{R_{\mathrm{s}}}\dfrac{R_{\mathrm{s}}^2}{r^2}+\dfrac{(1-\lambda)}{2}p_0\left(3\dfrac{R_{\mathrm{s}}^4}{r^4}-4\upsilon\dfrac{R_{\mathrm{s}}^2}{r^2}\right)\cos 2\theta\right] \end{cases} \tag{25}$$

5.3 Stress and deformation of plastic region

When r=R_{s}, the stress boundary condition is $\sigma_r^{\mathrm{s}}=\sigma_r^{R_{\mathrm{s}}}\big|_{r=R_{\mathrm{s}}}$. By substituting Eq.(14) into Eq.(20) and integrating, the stress of the plastic softening region can be obtained as:

$$\begin{cases} \sigma_r^{\mathrm{s}}=\left(\sigma_r^{R_{\mathrm{s}}}+\dfrac{B_{\mathrm{s}}}{A_{\mathrm{s}}-1}\right)\left(\dfrac{r}{R_{\mathrm{s}}}\right)^{A_{\mathrm{s}}-1}-\dfrac{B_{\mathrm{s}}}{A_{\mathrm{s}}-1} \\ \sigma_\theta^{\mathrm{s}}=A_{\mathrm{s}}\left(\sigma_r^{R_{\mathrm{s}}}+\dfrac{B_{\mathrm{s}}}{A_{\mathrm{s}}-1}\right)\left(\dfrac{r}{R_{\mathrm{s}}}\right)^{A_{\mathrm{s}}-1}-\dfrac{B_{\mathrm{s}}}{A_{\mathrm{s}}-1} \end{cases} \tag{26}$$

Based on elastic-plastic theory, the strain in the plastic softening region consists of two components: elastic strain and plastic strain. Then, the total strain can be expressed as:

$$\begin{Bmatrix} \varepsilon_r^{\mathrm{s}} \\ \varepsilon_\theta^{\mathrm{s}} \end{Bmatrix} = \begin{Bmatrix} \varepsilon_r^{\mathrm{se}} \\ \varepsilon_\theta^{\mathrm{se}} \end{Bmatrix} + \begin{Bmatrix} \varepsilon_r^{\mathrm{sp}} \\ \varepsilon_\theta^{\mathrm{sp}} \end{Bmatrix} \tag{27}$$

The elastic and plastic strains are represented by the superscript symbols "se" and "sp", respectively.

Considering the dilatancy effect of coal, the strain also can be expressed as:

$$g = \varepsilon_r^{\mathrm{s}} + A_{\mathrm{s}}^* \varepsilon_\theta^{\mathrm{s}} \tag{28}$$

By introducing Eq.(27) into Eq.(28), and satisfied the dilatancy condition Eq.(18), the strain can be written as:

$$g = \varepsilon_r^{\mathrm{se}} + A_{\mathrm{s}}^* \varepsilon_\theta^{\mathrm{se}} \tag{29}$$

When r=R_{s}, the strain boundary conditions are $\varepsilon_r^{\mathrm{se}} = \varepsilon_r^{\mathrm{e}}\big|_{r=R_{\mathrm{s}}}$ and $\varepsilon_\theta^{\mathrm{se}} = \varepsilon_\theta^{\mathrm{e}}\big|_{r=R_{\mathrm{s}}}$. Using the geometric equation Eq.(21), it can be obtained as:

$$g = \varepsilon_r^{\mathrm{se}} + A_{\mathrm{s}}^* \varepsilon_\theta^{\mathrm{se}} = \varepsilon_r^{\mathrm{e}}\big|_{r=R_{\mathrm{s}}} + A_{\mathrm{s}}^* \varepsilon_\theta^{\mathrm{e}}\big|_{r=R_{\mathrm{s}}} = \frac{\mathrm{d}u_s}{\mathrm{d}r} + A_{\mathrm{s}}^* \frac{u_s}{r} \tag{30}$$

When r=R_{s}, the displacement boundary condition is $u_{\mathrm{s}} = u_{\mathrm{e}}\big|_{r=R_{\mathrm{s}}}$. Then, the displacement and strain solutions can be obtained through the integration of the geometric equation combined with the dilatancy model, and it is expressed as:

$$\begin{cases} u_{\mathrm{s}} = \dfrac{Mr}{A_{\mathrm{s}}^* + 1}\left[1 - \left(\dfrac{R_{\mathrm{s}}}{r}\right)^{A_{\mathrm{s}}^*+1}\right] + Nr\left(\dfrac{R_{\mathrm{s}}}{r}\right)^{A_{\mathrm{s}}^*+1} \\ \varepsilon_r^{\mathrm{s}} = \dfrac{M}{A_{\mathrm{s}}^* + 1}\left[1 + A_{\mathrm{s}}^*\left(\dfrac{R_{\mathrm{s}}}{r}\right)^{A_{\mathrm{s}}^*+1}\right] - A_{\mathrm{s}}^* N\left(\dfrac{R_{\mathrm{s}}}{r}\right)^{A_{\mathrm{s}}^*+1} \\ \varepsilon_\theta^{\mathrm{s}} = \dfrac{M}{A_{\mathrm{s}}^* + 1}\left[1 - \left(\dfrac{R_{\mathrm{s}}}{r}\right)^{A_{\mathrm{s}}^*+1}\right] + N\left(\dfrac{R_{\mathrm{s}}}{r}\right)^{A_{\mathrm{s}}^*+1} \end{cases} \tag{31}$$

M and N are the calculation coefficients, which can be expressed as:

$$\begin{cases} M = \dfrac{1+\upsilon}{E}\left\{\dfrac{(1+\lambda)}{2} p_0\left(A_{\mathrm{s}}^* - 1\right) - \sigma_r^{R_{\mathrm{s}}}\left(A_{\mathrm{s}}^* - 1\right) + \dfrac{(1-\lambda)}{2} p_0\left[A_{\mathrm{s}}^*(3-4\upsilon) - (4\upsilon - 1)\right]\cos 2\theta\right\} \\ N = \dfrac{1+\upsilon}{E}\left[\dfrac{(1+\lambda)}{2} p_0 - \sigma_r^{R_{\mathrm{s}}} + \dfrac{(1-\lambda)}{2} p_0 (3-4\upsilon)\cos 2\theta\right] \end{cases}$$

5.4 Stress and deformation of broken region

When r=R_0, the stress boundary condition is $\sigma_r^b\big|_{r=R_0} = 0$. By introducing Eq.(14) into Eq.(20) and integrating, the stress can be calculated as:

$$\begin{cases} \sigma_r^{\mathrm{b}} = \dfrac{B_{\mathrm{b}}}{A_{\mathrm{b}}-1}\left[\left(\dfrac{r}{R_0}\right)^{A_{\mathrm{b}}-1}-1\right] \\ \sigma_\theta^{\mathrm{b}} = \dfrac{A_{\mathrm{b}}B_{\mathrm{b}}}{A_{\mathrm{b}}-1}\left[\left(\dfrac{r}{R_0}\right)^{A_{\mathrm{b}}-1}-1\right]+B_{\mathrm{b}} \end{cases} \tag{32}$$

Similarly, the calculation process is completely consistent with the plastic softening region, and when $r=R_{\mathrm{b}}$, the strain and displacement boundary conditions are $\varepsilon_r^{\mathrm{be}} = \varepsilon_r^{\mathrm{s}}\big|_{r=R_{\mathrm{b}}}$, $\varepsilon_\theta^{\mathrm{be}} = \varepsilon_\theta^{\mathrm{s}}\big|_{r=R_{\mathrm{b}}}$, and $u_{\mathrm{b}} = u_{\mathrm{s}}\big|_{r=R_{\mathrm{b}}}$, respectively. Thus, the displacement and strain solutions can be derived as:

$$\begin{cases} u_{\mathrm{b}} = \dfrac{Cr}{A_{\mathrm{b}}^*+1}\left[1-\left(\dfrac{R_{\mathrm{b}}}{r}\right)^{A_{\mathrm{b}}^*+1}\right]+\dfrac{Mr}{A_{\mathrm{s}}^*+1}\left[1-\left(\dfrac{R_{\mathrm{s}}}{R_{\mathrm{b}}}\right)^{A_{\mathrm{s}}^*+1}\right]\left(\dfrac{R_{\mathrm{b}}}{r}\right)^{A_{\mathrm{b}}^*}+NR_{\mathrm{b}}\left(\dfrac{R_{\mathrm{s}}}{R_{\mathrm{b}}}\right)^{A_{\mathrm{s}}^*+1}\left(\dfrac{R_{\mathrm{b}}}{r}\right)^{A_{\mathrm{b}}^*} \\ \varepsilon_r^{\mathrm{b}} = \dfrac{C}{A_{\mathrm{b}}^*+1}\left[1+A_{\mathrm{b}}^*\left(\dfrac{R_{\mathrm{b}}}{r}\right)^{A_{\mathrm{b}}^*+1}\right]+\dfrac{M}{A_{\mathrm{s}}^*+1}\left(1-A_{\mathrm{b}}^*\right)\left[1-\left(\dfrac{R_{\mathrm{s}}}{R_{\mathrm{b}}}\right)^{A_{\mathrm{s}}^*+1}\right]\left(\dfrac{R_{\mathrm{b}}}{r}\right)^{A_{\mathrm{b}}^*}-A_{\mathrm{b}}^*N\left(\dfrac{R_{\mathrm{s}}}{R_{\mathrm{b}}}\right)^{A_{\mathrm{s}}^*+1}\left(\dfrac{R_{\mathrm{b}}}{r}\right)^{A_{\mathrm{b}}^*+1} \\ \varepsilon_\theta^{\mathrm{b}} = \dfrac{C}{A_{\mathrm{b}}^*+1}\left[1-\left(\dfrac{R_{\mathrm{b}}}{r}\right)^{A_{\mathrm{b}}^*+1}\right]+\dfrac{M}{A_{\mathrm{s}}^*+1}\left[1-\left(\dfrac{R_{\mathrm{s}}}{R_{\mathrm{b}}}\right)^{A_{\mathrm{s}}^*+1}\right]\left(\dfrac{R_{\mathrm{b}}}{r}\right)^{A_{\mathrm{b}}^*}+N\left(\dfrac{R_{\mathrm{s}}}{R_{\mathrm{b}}}\right)^{A_{\mathrm{s}}^*+1}\left(\dfrac{R_{\mathrm{b}}}{r}\right)^{A_{\mathrm{b}}^*+1} \end{cases} \tag{33}$$

C is the calculation coefficient, which can be given as:

$$C = \frac{A}{A_{\mathrm{s}}^*+1}\left[\left(1+A_{\mathrm{b}}^*\right)+\left(A_{\mathrm{s}}^*-A_{\mathrm{b}}^*\right)\left(\frac{R_{\mathrm{s}}}{R_{\mathrm{b}}}\right)^{A_{\mathrm{s}}^*+1}\right]+\left(A_{\mathrm{b}}^*-A_{\mathrm{s}}^*\right)N\left(\frac{R_{\mathrm{s}}}{R_{\mathrm{b}}}\right)^{A_{\mathrm{s}}^*+1}$$

5.5 Solution of radii (R_{s} and R_{b})

When $r=R_{\mathrm{b}}$, the stress boundary is $\sigma_r^{\mathrm{s}} = \sigma_r^{\mathrm{b}}\big|_{r=R_{\mathrm{b}}}$. The relationship between R_{s} and R_0 can be derived as:

$$R_{\mathrm{s}} = R_0\left[1+\frac{\sigma_r^{R_{\mathrm{s}}}\left(A_{\mathrm{b}}-1\right)}{B_{\mathrm{b}}}\right]^{\frac{1}{A_{\mathrm{b}}-1}} \tag{34}$$

6 Validation of the distribution laws of stress and deformation

To investigate the laws of stress and deformation in the plastic region, a numerical analysis model of the coal after drilling under plane strain conditions is established, and the shape and size of the plastic region are compared between the analytical and numerical results. The simulation was performed by using the finite element analysis software (ANSYS), with the DP strength criterion adopted for the analysis. During the numerical analysis process, a strength parameter softening model specific to coal was redefined and integrated into the software to ensure consistency with the analytical framework. Specifically, referring to earlier studies (Deng et al. 2018; Han et al. 2013), the strength parameter relationships described in Eq.(5) and Eq.(6) were incorporated into the numerical analysis, which can reflect the reduction in coal strength parameters as the yield process progresses.

In this section, a simple example is presented. The borehole diameter is 0.1m, and the parameters of coal used in the numerical analysis as follows: the vertical stress p_0=10MPa, the horizontal stress λp_0=12MPa, the ration of horizontal to vertical stress is λ=1.2, the unit weight of coal is γ=14kN/m^3, the Elastic modulus is E=1.05GPa, the Poisson's ratio υ=0.35, the Peak cohesion c_{p}=3.0MPa, and the Peak internal friction angle φ_{p}=30°, respectively.

According to the load-bearing characteristics of the borehole surrounding coal, the numerical model can be treated as a two-dimensional plane strain problem. The size of geometric model is 3×3m, and the borehole is centrally located

for the convenience of numerical calculation. It can be seen that the ratio of the model side length to the borehole diameter is 30:1, which is favorable for diminishing the effect of the boundary. Considering the stress concentration induced by borehole drilling, the density of computational elements decreases gradually forms the geometric model center to its periphery. Additionally, the meshing scheme is considered reasonable if, after refining the mesh by 10%, the change in the maximum deformation value does not exceed 1%. The finite element model consisted of 6146 (8-noded quadrangular node) elements and 18630 nodes in total, which ensured the reliability of the calculation results. The boundary conditions are defined as follows: the top of the model is a free boundary (all displacements unconstrained); both sides of the model are constrained horizontally (u_x=0), but free vertically (u_y unconstrained); the bottom of the model is subjected to a fully fixed constraint (u_x=u_y=0). The geometry of the finite element model, mesh configuration, and corresponding boundary conditions in the Cartesian coordinate system are displayed in Figure 8.

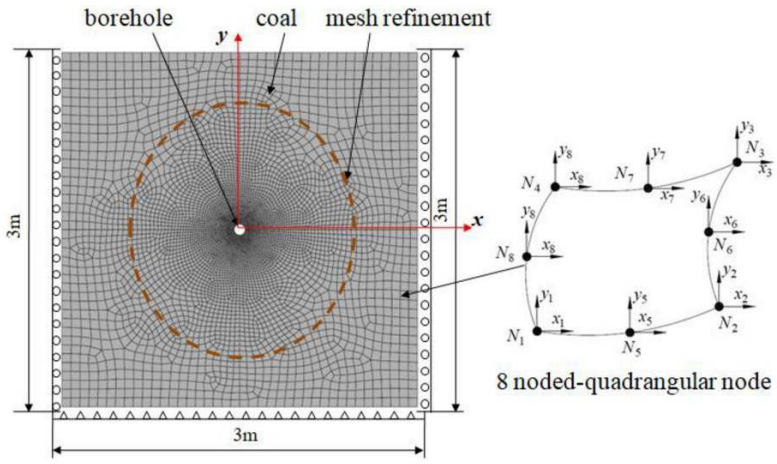


Figure 8 Numerical model and boundary conditions

6.1 Influence of strength parameters on distribution of stress and deformation

Zhang et al. (2025) previously conducted a detailed discussion the effects of various parameters such as lateral pressure coefficient, vertical stress, borehole radius, and intermediate principal stress coefficient on the radius of different deformation regions, so the influences of residual strength parameters on the distribution of stress and deformation with the plastic region will be mainly studied in this work. In fact, the plastic region can reflect the maximum failure tolerance of the coal surrounding borehole to failure risks. Therefore, the relationship between the changed strength parameters and the shape and size of the plastic region will be the focus in this section.

6.1.1 Influence of cohesion on distribution of stress and deformation

To study the effect of residual cohesion on the shape and size of the plastic region, the residual cohesion values are selected as 3.0, 2.0, 1.0, and 0.5MPa, respectively, and other parameters remain the same. The analytical result is shown in Figure 9. It can be found that the plastic region distribution appears more likely to be peanut-shaped with decreasing residual cohesion, which that the deformation on both sides of the borehole is small, while the deformation at the top and bottom parts is large. The shape and size of the plastic region increase gradually as the residual cohesion decreases, and the lower the residual cohesion, the larger the plastic region. Also, when the residual cohesion values are 3.0, 2.0, 1.0, and 0.5MPa, the major axis radii of the plastic region are 0.088, 0.106, 0.140, and 0.196m, and the minor radii of the plastic region are 0.057, 0.061, 0.070, and 0.086m, respectively. Obviously, the top and bottom regions of the borehole exhibit the poorest safety and reliability compared with other locations, a phenomenon that is associated with the lateral pressure coefficient λ. If λ<0, the result is opposite (Fan et al, 2020; Xu et al, 2023; Zhang et al, 2025). Thus, the shape of the plastic region is governed by the lateral pressure coefficient, while the reduction in residual cohesion intensifies the concave deformation on both sides. In fact, when c_r=3.0MPa, it implies that the plastic softening behavior is not taken into account. However, this assumption is inconsistent with the actual conditions, as Table 1 clearly shows that the average rate of change of cohesion is 53.87%, which directly contradicts the conclusion that the cohesion is unchanging. It will seriously underestimate the distribution and size of the plastic softening region, which could lead to a misjudgment about the safety of the coal surrounding borehole. Therefore, as a critical strength parameter, the softening behavior of cohesion must be considered in analysis.

Figure 10 illustrates the variation rule of the plastic radius with the polar angle in first quadrant. It is evident that the plastic radius exhibits a nonlinear increase with an increase in the polar angle, and the entire process can be simplified as a combination of three linear parts. The polar angle 0~30° is part I, 30~60° is part II, and 60~90° is part III. As an illustration, for c_r=0.5MPa, the gradient of part II is the largest, indicating that the plastic deformation extends most rapidly. This mechanism is of great significance in studying the deformation characteristics of the coal surrounding borehole. As reported in relevant published studies, a large lateral pressure coefficient significantly alters the size and shape of the plastic deformation region, leading to the formation of an X-shaped pattern (Zheng et al. 2012; Geng et al. 2023; Jin et al. 2021). The maximum plastic radius is exactly observed in Part II, which coincides with the maximum gradient of plastic deformation. Under general geological conditions, the confining pressure ratio of coal around borehole in the stress field (i.e., λ=1.0~2.0) gradually approaches 1.0 with increasing burial depth. Hence, the peanut-shaped deformation pattern is of great practical significance. Furthermore, it can also be inferred that the shape of the plastic region is circular when λ=1.0.

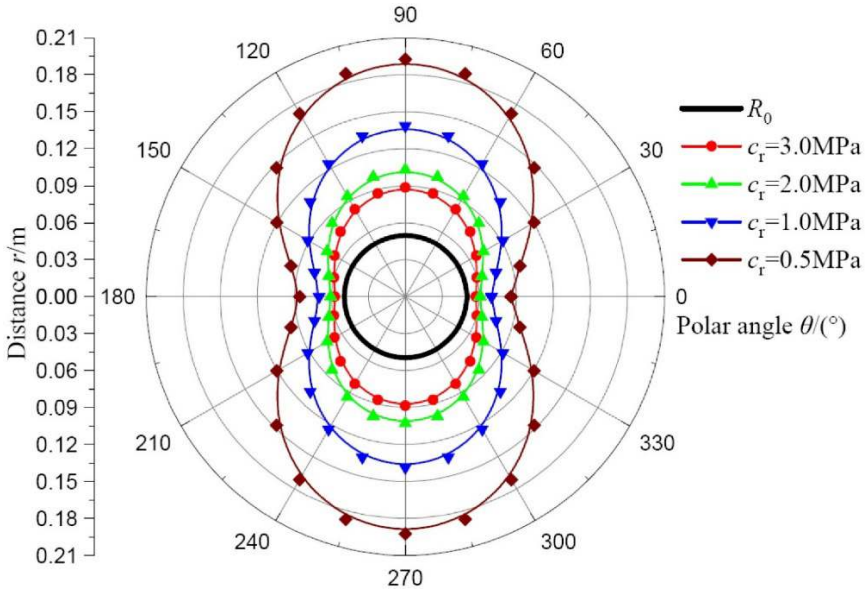


Figure 9 Plastic region distribution under different residual cohesion in analytical method

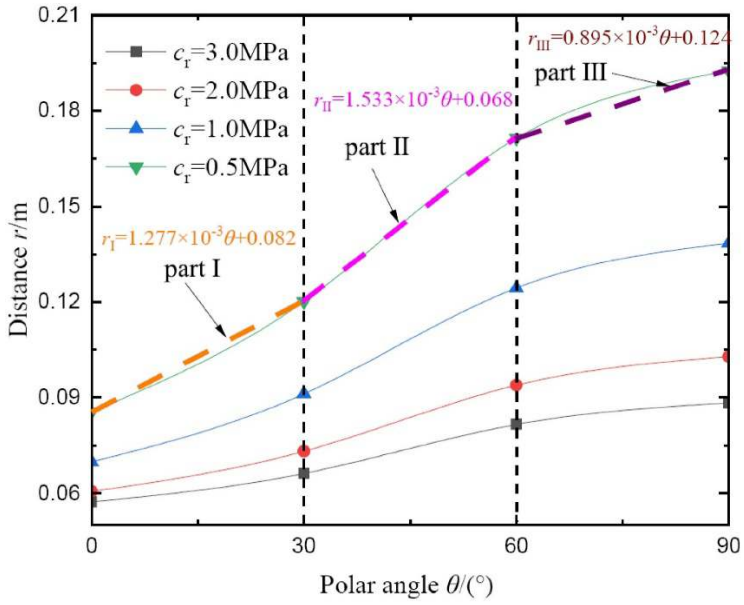


Figure 10 The change rule of plastic radius with polar angle

Figure 11 presents the distribution of the plastic region under different residual cohesion conditions. For the same residual cohesion, the maximum deformation also occurs at the top and bottom of the coal surrounding of borehole. The

process of deformation extension indicates that residual cohesion affects the top and bottom of borehole first, followed by its two sides. Based on the numerical simulation results, the major axis radii of the plastic region are 0.096, 0.114, 0.155, and 0.218m, corresponding to residual cohesions of 3.0, 2.0, 1.0, and 0.5MPa, respectively. Overall, the numerical results are slightly larger than the analytical results. The relative errors between the numerical simulation results and analytical solutions are 9.01, 7.54, 10.71, and 11.22%, respectively, with the maximum error value being less than 12%, which further verifies the reliability of the numerical simulation method. This error can be attributed to the differences of the calculation methods. In the analytical method, although the calculated results are based on the strict assumptions and boundary conditions, it can still describe some general rules governing the deformation distribution within the plastic region. Numerical simulation is capable of depicting the intrinsic response characteristics of complex deformation processes and objectively determining the stress and deformation trends in the coal surrounding borehole. Thus, although the results obtained by two aforementioned methods exhibit slight discrepancies, the trends of deformation distribution within the plastic region are consistent.

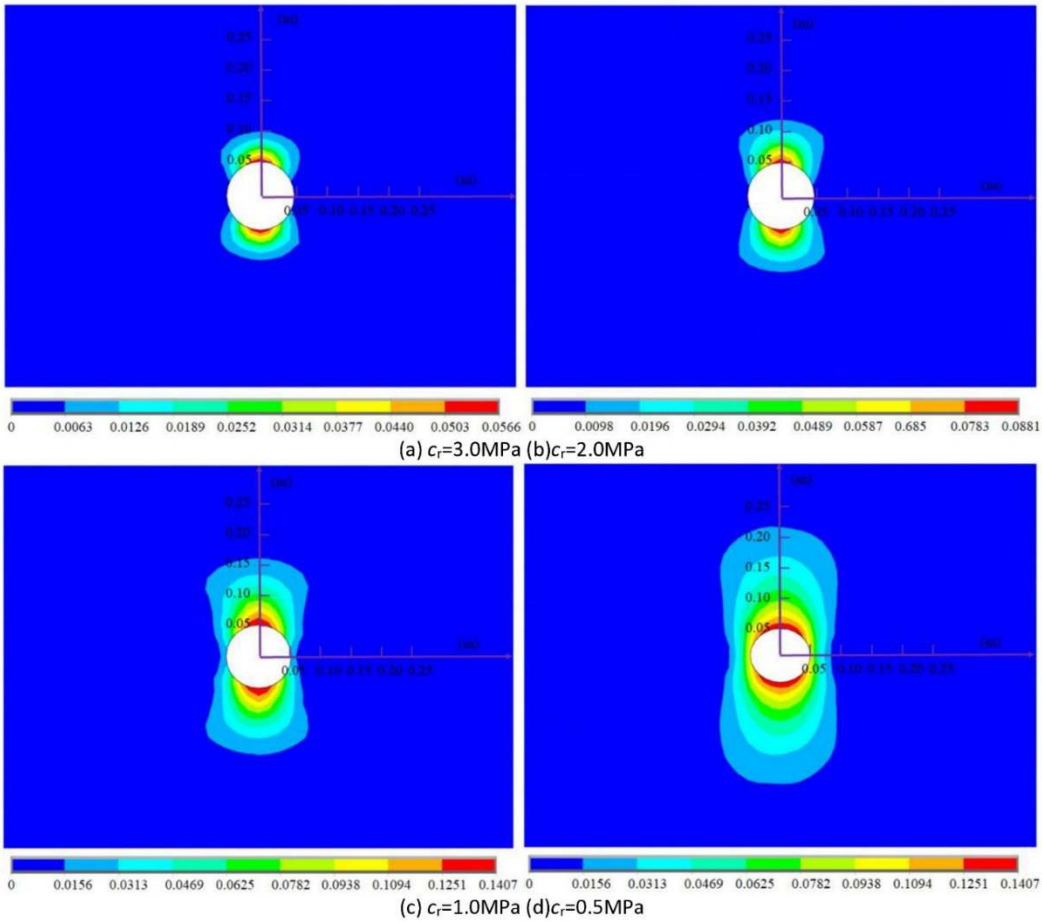
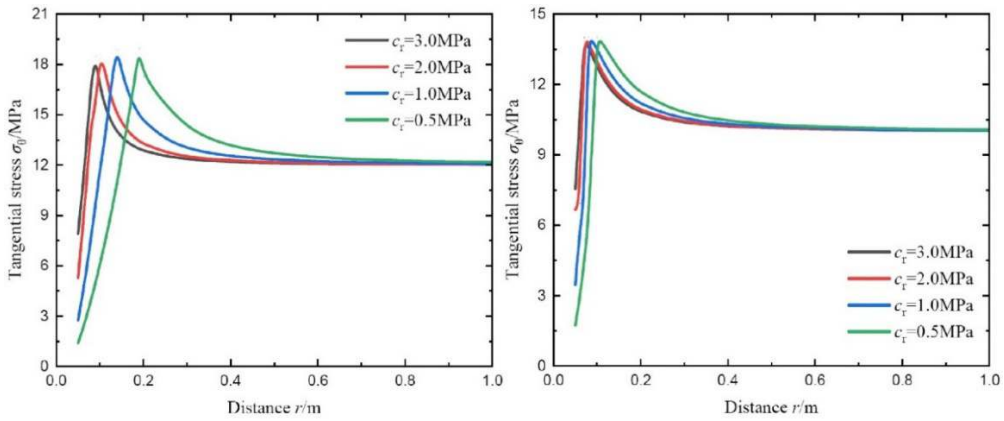


Figure 11 Plastic region distribution under different residual cohesion in numerical calculation

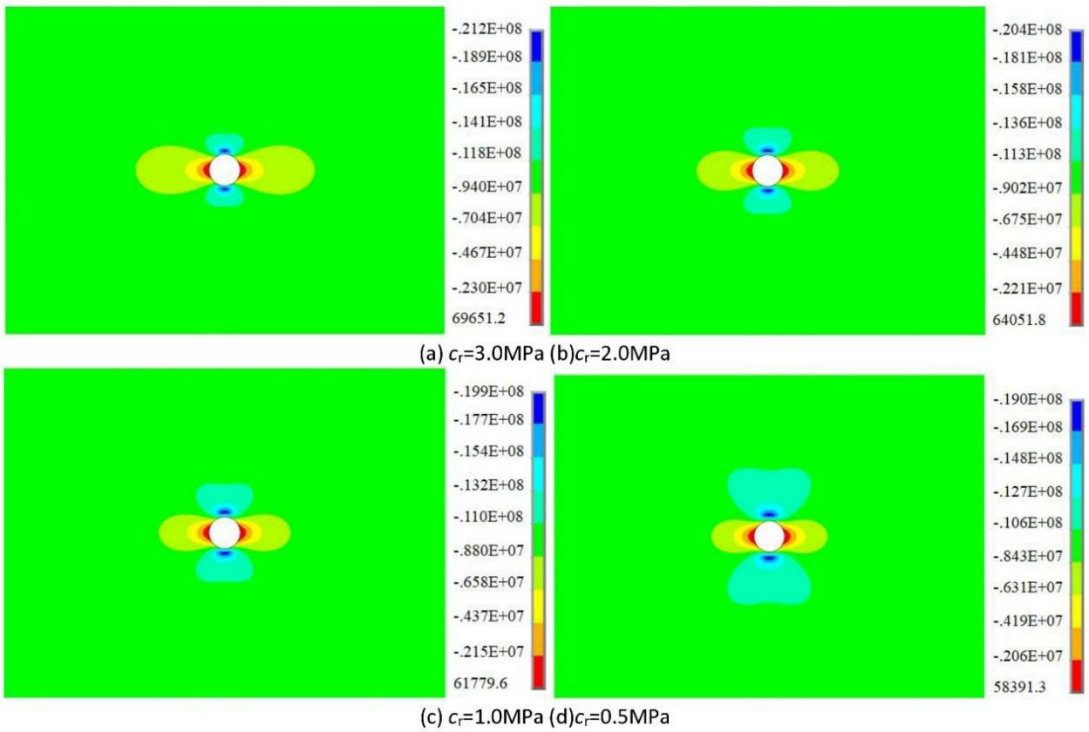
Figure 12 shows the analytical solutions of the tangential stress at ϑ=90° and 0°. It can be clearly found that the tangential stress initially increases with the distance from the borehole center, then decreases as the distance future increases, and eventually stabilizes at a constant value. Although the maximum stress values are essentially identical, the corresponding locations gradually shift farther from the borehole center as the residual cohesion decreases. It also indicates that the expansion rate of vertical plastic region is faster than that of the horizontal plastic region. Based on elastic-plastic theory, the post-peak tangential stress region undergoes elastic deformation. Hence, the plastic region is located within the pre-peak stress stage, which is consistent with the plastic radius distribution under different residual cohesion values. Moreover, the peak tangential stress at ϑ=90° is 18.47MPa, approximately 1.33 times that the value at ϑ=0°. Therefore, the top and bottom of the coal surrounding borehole suffer more severe rupture than the two sides. Additionally, when the distance to the center of the borehole is r=1.0m, namely the ratio of the calculated length to the borehole diameter is 10:1, the stress remains essentially unchanged, which indicates that the finite element numerical model is reasonable.

Figure 13 describes the numerical results of the vertical stress fields surrounding the borehole. It can be observed that the vertical stresses surrounding the borehole are symmetrically distributed, and the maximum stress values are also essentially identical under different residual values. The maximum stress value, approximately 20.0MPa, is located at the top and bottom of the borehole. Meanwhile, the primary plastic region is also located at the top and bottom of the borehole, and expands upward and downward as the residual cohesion decreases. Considering the effect of the lateral pressure coefficient λ>1.0, the horizontal deformation within the plastic region shows an obvious attenuation. It also indicates that the top and bottom of the borehole are more prone to damage than the sides, and that the smaller the residual cohesion, the larger the damage region. In terms of the stress concentration, vertical stress concentration degree is also higher than horizontal stress concentration. When the lateral pressure coefficient λ>1.0, the horizontal stress exceeds the vertical stress. Correspondingly, two sides of the borehole exhibit a remarkable depression, which is illustrated in Figure 9 and Figure 11. For this reason, vertical deformation is constrained by the overlying strata during the borehole enlargement process, leaving minimal deformation space and thus intensifying stress concentration. Consequently, the top and bottom of the borehole become the most severely damaged regions as the damage process progresses under these conditions.



(a) ϑ=90° (b) ϑ=0°

Figure 12 Tangential stress results calculated by analytical method



(a) c_r=3.0MPa (b)c_r=2.0MPa

(c) c_r=1.0MPa (d)c_r=0.5MPa

Figure 13 Vertical stress distribution of the coal around borehole

Figure 14 presents the tangential stress results from the analytical solutions and numerical simulation at ϑ=90° and 0°. It can be seen that the results of the simulation compared reasonably well to the analytical results in terms of the stress profiles along the same monitoring path. The stress curves follow almost the same laws along the radial direction in spite of the differences in residual cohesion. Overall, the simulation results are relatively small in comparison to the analytical results. When the residual cohesion is 3.0MPa, it represents that the strain-softening is not considered. The correlation coefficient between the analytical results and numerical simulations is 0.96 with a stress error of 6.43%, indicating the best performance among all comparative analyses. As residual cohesion decreases, the error in stress exhibits a distinct increase trend. Based on the statistical analysis of the data, when the residual cohesion is 0.5MPa, the maximum stress error reaches 11.72%, while the minimum correlation coefficient is 0.89. In view of the complexity of deep coal and rock mass, a stress error 10%-15% is considered acceptable in engineering practice (Zheng et al. 2012). Thus, the two methods also enhance the validity and reliability of the analysis findings through mutual verification.

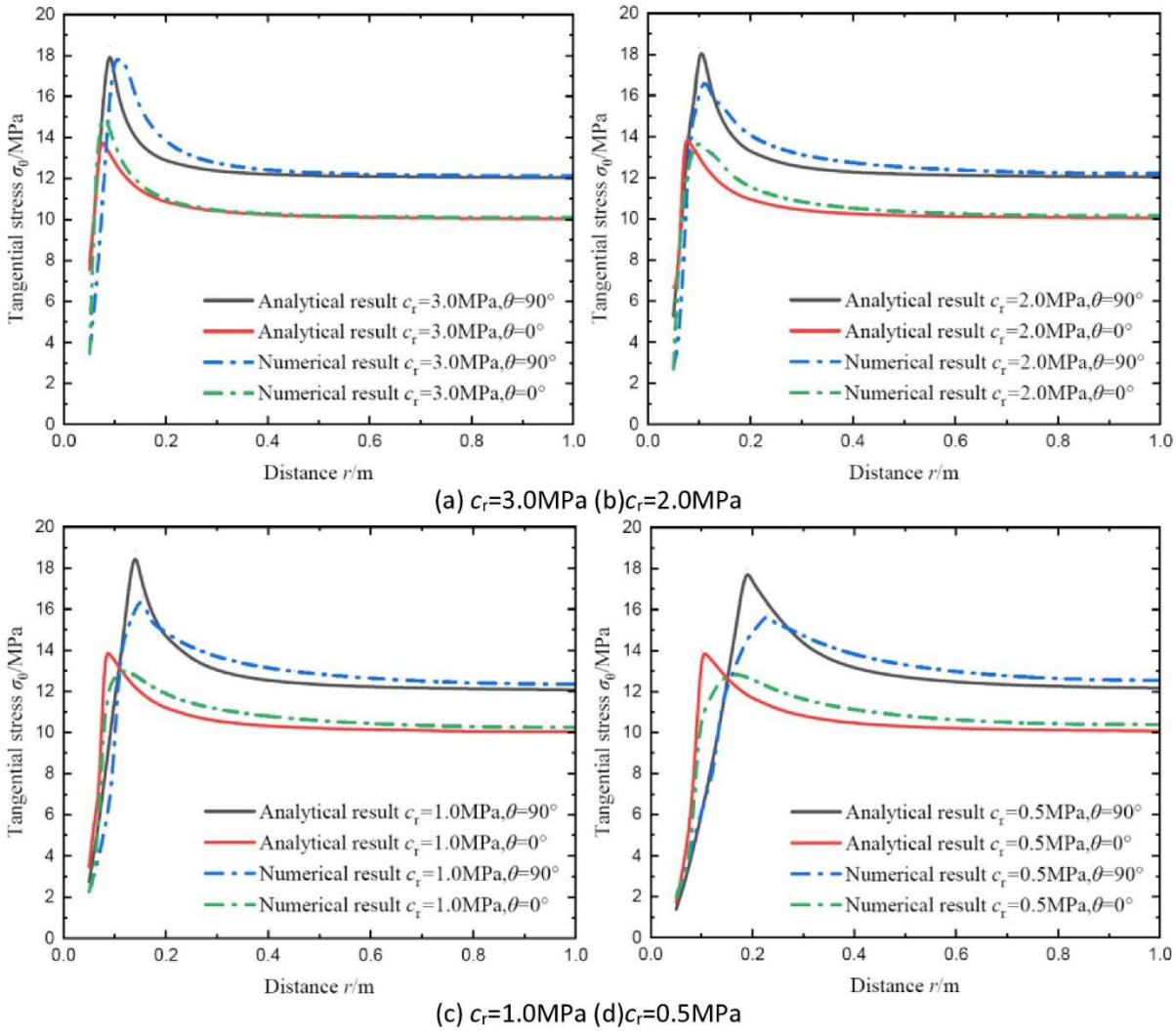


Figure 14 Tangential stress for different methods

6.1.2 Influence of internal friction angle on distribution of stress and deformation

Table1 shows that the internal friction angle is not invariable, and it also it also exerts a certain strain-softening significance effect on the strength properties of the coal. Thus, it is highly necessary to identify the relationship between the residual internal friction angle and the plastic deformation of the coal surrounding borehole. In this section, the residual internal friction angle values are selected as 30, 25, 20, and 15°, respectively, and the cohesion value is set as 3.0MPa. Figure 15 presents the distributions of plastic regions with various residual internal friction angles obtained by an analytical method. Similar to Figure 9, the plastic region also exhibits a peanut-shaped. As the residual internal friction angle decreases, the increase rate of the vertical plastic radius is significantly higher than that of horizontal plastic radius.

The smaller the residual internal friction angle, the larger the plastic region radius becomes. For instance, when the residual internal friction angle values are 30, 25, 20, and 15°, the major axis plastic region radius increases by 55.67% (from 0.088m to 0.137m), but the minor axis plastic region radius increases by only 7.02% (from 0.057m to 0.061m). That is a nearly 8 times difference in change rate of the plastic region radius between the two directions. In terms of plastic region size, the results indicate that the plastic radius affected by the residual internal friction angle is smaller than that affected by the residual cohesion. Although the residual cohesion plays a dominant role in the distribution of plastic regions, the residual internal friction angle also exerts a certain influence on their expansion. Obviously, neglecting the effect of the residual internal friction angle on the plastic deformation region will induce discrepancies between theoretical models and practical engineering results.

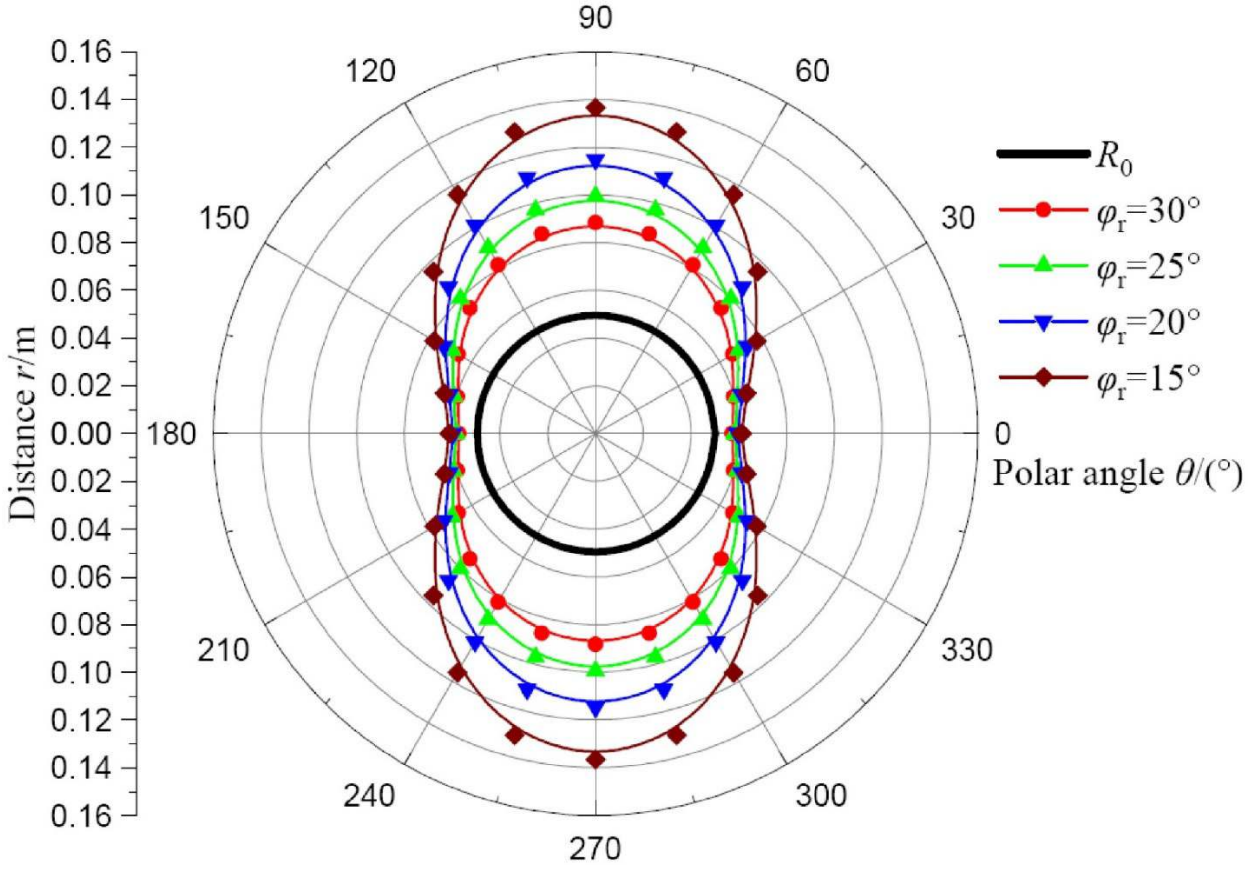


Figure 15 Plastic region distribution in analytical method

Figure 16 shows the plastic region distribution under different residual internal friction angle. It can be observed that the major axis radii of the plastic region are 0.096, 0.102, 0.118, and 0.141m, while the residual internal friction angles are 30, 25, 20, and 15°, respectively. Comparatively, the analytical solutions are 0.088, 0.099, 0.115, and 0.137m, respectively. The maximum error value is 9.09%, which further confirms the practicality and effectiveness of both the analytical method and numerical simulation method. In general, the plastic softening effect induced by cohesion is more pronounced than that induced by the internal friction angle. For instance, in the numerical results, when the reduction ratio of the two strength parameters is the same (i.e., the residual cohesion decreases from 3.0MPa to 2.0MPa and the residual friction angle decreases from 30° to 20°), the corresponding plastic region radii are 0.155m and 0.118m, respectively. It should be noted that this conclusion is derived solely from a single strength parameter softening, but if both parameters undergo simultaneously softening, the plastic region will expand to a larger extent.

To verify the reliability of the analytical method, the result with a residual internal friction angle φ_r=25° is taken as an example. The radial and tangential results obtained from the analytical and numerical methods are compared in Figure 17. It shows that these two methods yield similar stress distributions, and the relative error is also limited to 10%. Therefore, regardless of variations in the strength parameters, the results obtained from the two aforementioned methods remain reliable.

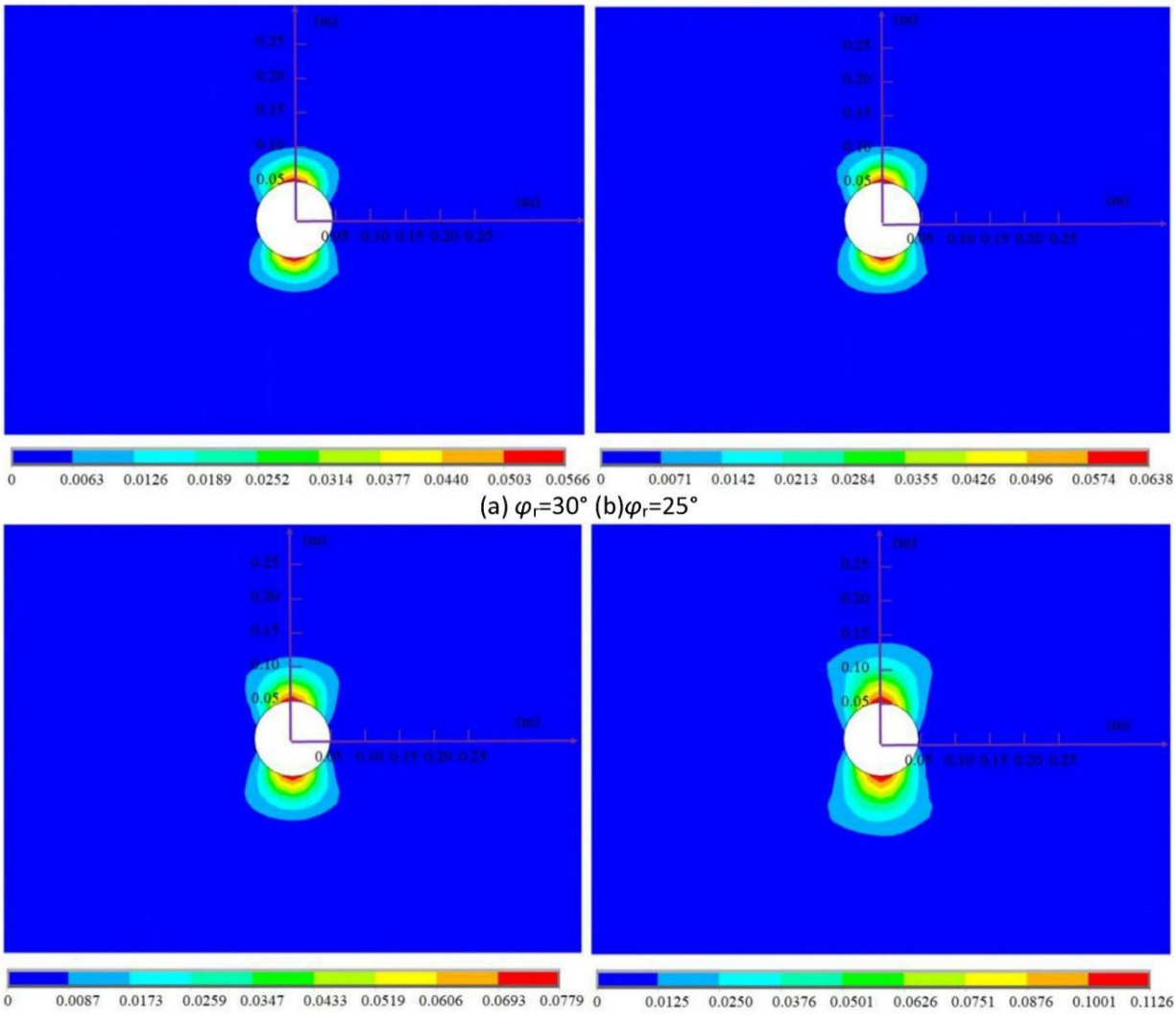
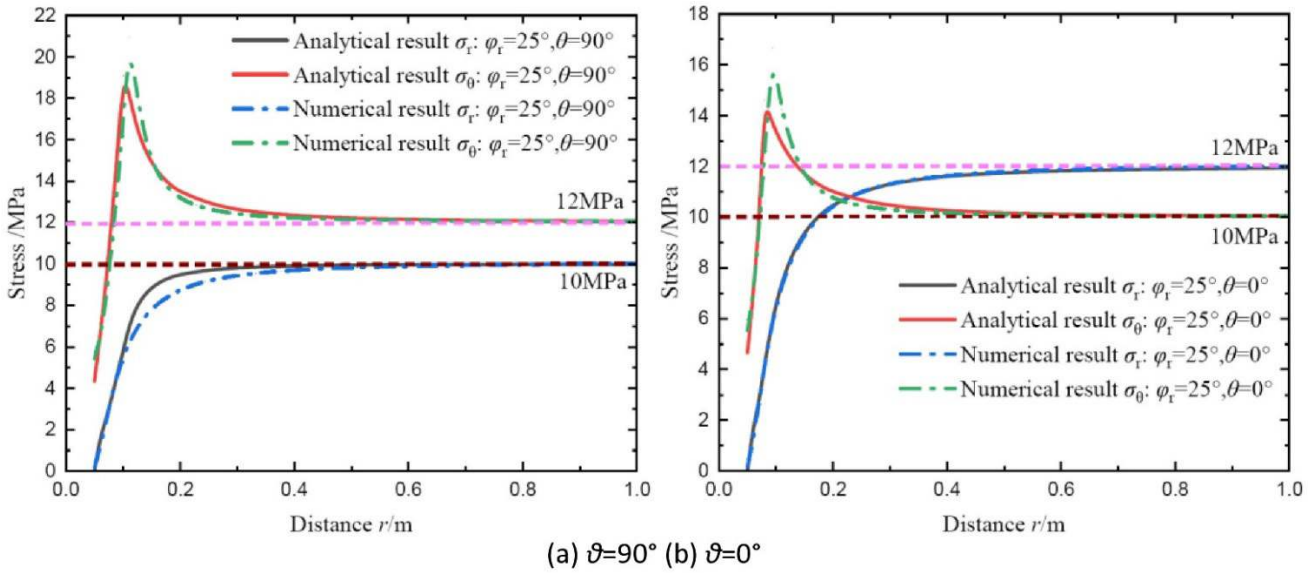


Figure 16 Plastic region distribution in numerical calculation



(a) ϑ=90° (b) ϑ=0°

Figure 17 Radial and tangential stress for different methods

In order to better understand the evolution law of the plastic region with residual strength parameters, the spatial distribution of plastic region radii at ϑ=90° and ϑ=0° under the interaction of the two aforementioned parameters is presented in Figure 18. It can be seen that the influence of residual cohesion on the plastic region radii is prominently greater than that of the residual fiction angle, so the residual cohesion plays a vitally important role in the deformation distribution within the plastic region. Additionally, the attenuation of strength parameters is the key factor restricting the size of the plastic region, and the softening coefficient cannot be assigned arbitrarily. For instance, when the plastic softening of both parameters is all considered, the maximum plastic region radius is 0.929m, which is 18.58 times the borehole radius. This result is inconsistent with the experimental observations and theoretical expectations. Hence, the quantitative softening attenuation of strength parameters requires further triaxial tests for determination.

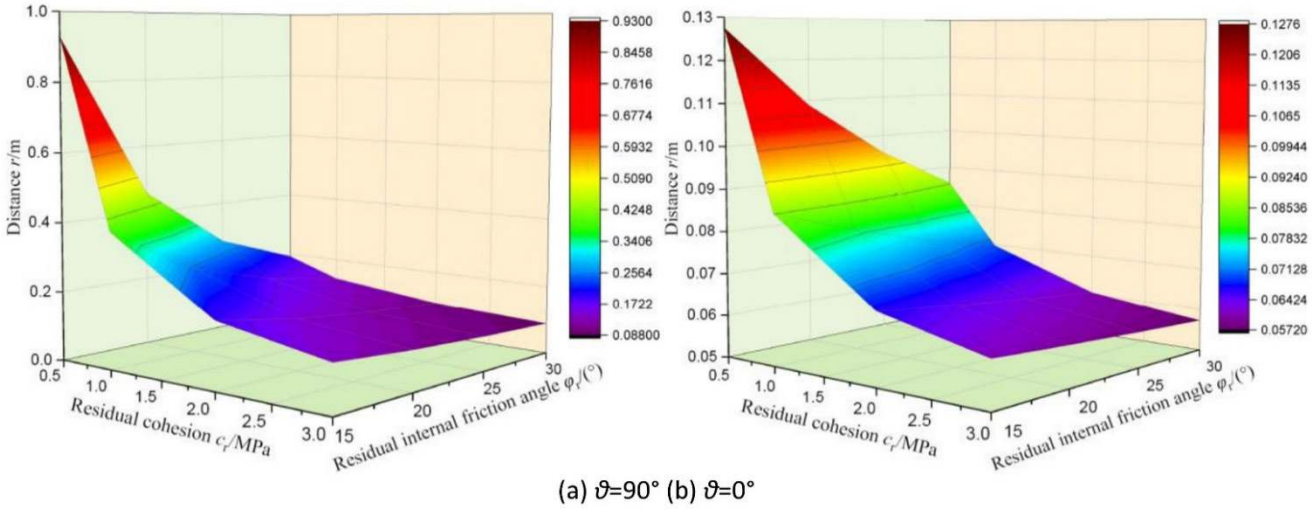


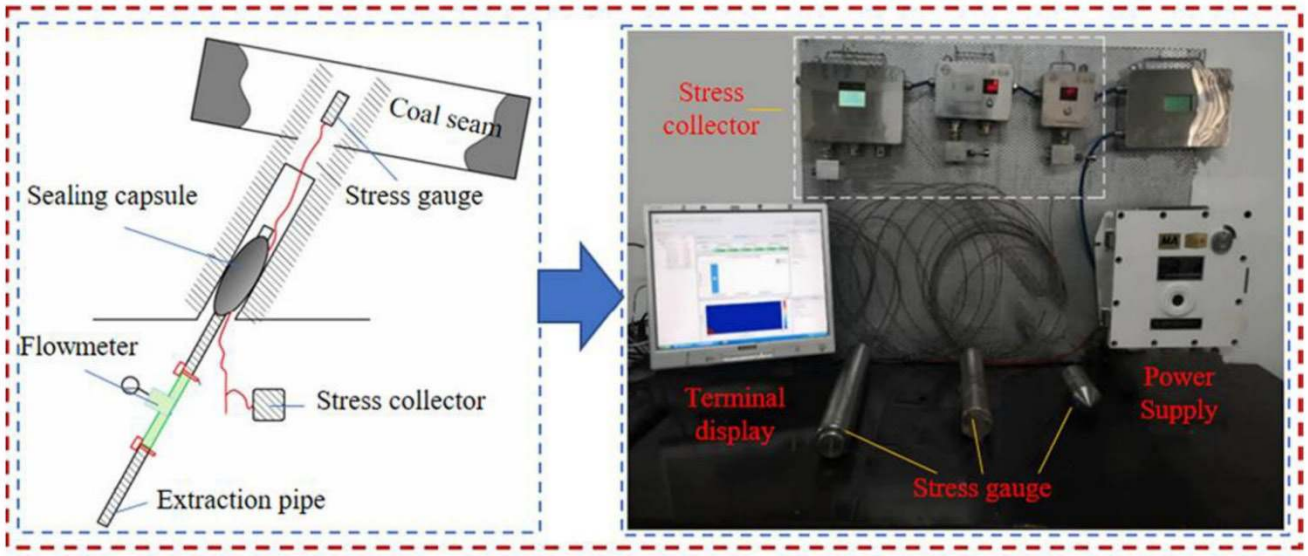
Figure 18 Effect of strength parameters interaction on plastic region

Through the analysis of theoretical and numerical simulation results, the distribution of stress and deformation in the plastic region is strongly affected by the residual strength parameters, so it is necessary to consider the strain softening effects of the strength parameters. It is important to note that the influence of the residual internal friction angle is not fixed, and its degree of influence needs to be determined through experiments. If the residual internal angle is not considered, the magnitude of deformation surrounding the borehole may be underestimated.

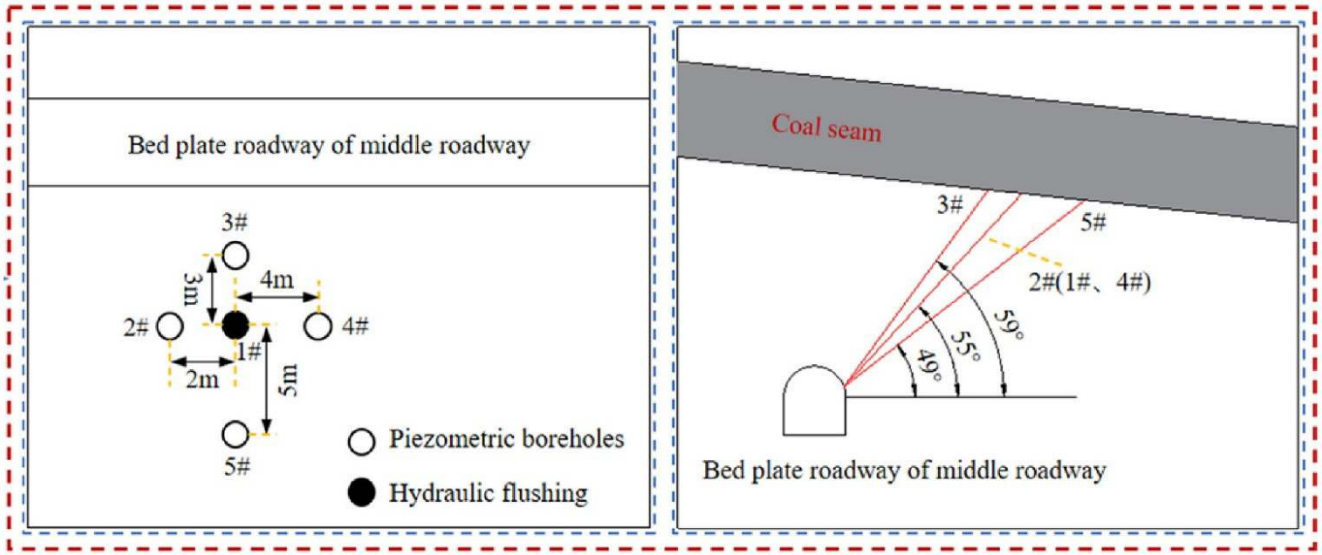
7 Field verification of the deformation distribution around borehole

In this section, the No.21 outburst coal seams of Liangbei coal mine in Henan Province is taken as the engineering background. The magnitude of coal deformation around the borehole has been investigated by several scholars including Wang et al. (2020) and Cui et al. (2023). Unfortunately, the plastic softening behavior of the internal friction angle was not taken into account in the aforementioned studies. Therefore, the effects of the softening characteristics of the two strength parameters on the deformation field will be discussed in detail in this section. The measuring equipment, installation method, and measuring point layout are shown in Figure 19. According to the test data, the physical parameters of the coal sample are presented as follows: the horizontal and vertical stress of coal seam is p_0=7.0MPa (λ=1.0), the elastic modulus is E=1.2GPa, the peak cohesion is c_p=1.5MPa, the peak internal friction angle is φ_p=20°, the density is ρ=1440 kg/m^3, the Poisson's ratio is υ=0.46, and the borehole radius is R_0=0.4m.

Based on the measured data, Wang et al (2020) identified three deformation zones, namely the stress reduction zone, the stress transition zone and the stress concentration zone. Taking the borehole center as the origin, the stress reduction zone is within 4m of the center, the stress transition zone is between 4m and 5m, and the stress concentration zone lies beyond 5m, as shown in Figure 20. According to the stress-strain relationship of the coal around borehole, the stress reduction zone, the stress transition zone, and the stress concentration zone correspond to the broken region, the plastic softening region and elastic region, respectively. This is consistent with the theoretical analytical model for area surrounding the borehole after construction, as shown in Figure 7. It can be inferred that the stress transition zone, also referred to as the plastic deformation zone, has a radius 12.5 times that of the borehole.



(a) Measuring equipment and installation method



(b) Measuring point location

Figure 19 Measuring equipment and measuring point location (Wang et al. 2020; Cui et al. 2023)

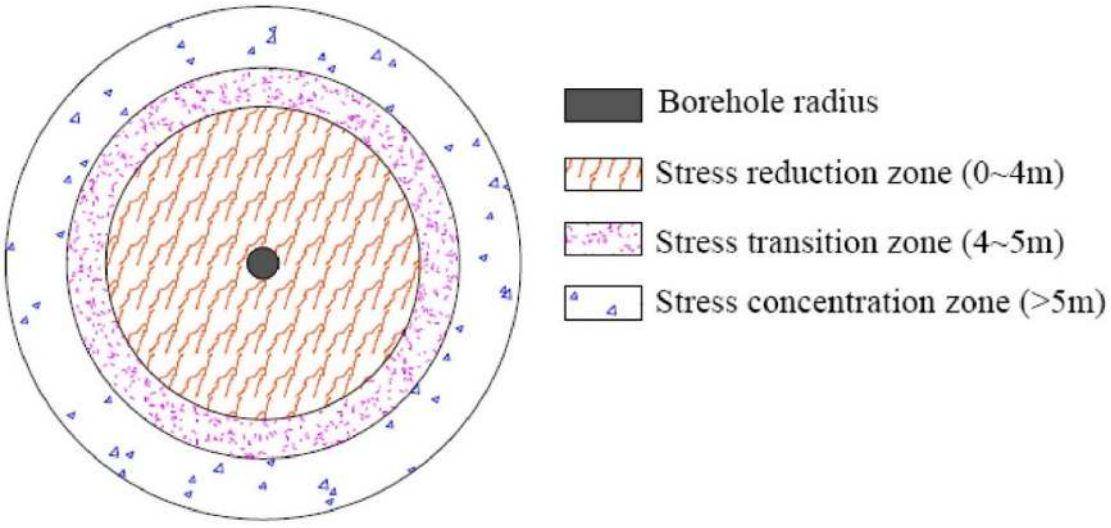


Figure 20 Stress distribution zones surrounding the borehole

If the plastic softening parameters are not considered (c_r=c_p=1.5MPa, φ_r=φ_p=20°), the plastic region radius is only 0.79m, which is 1.975 times the borehole radius. This result is seriously inconsistent with the field test data. Cui et al. (2023) assumed that the residual cohesion was reduced by 95% relative to the peak cohesion, whereas the internal friction angle remained unchanged. In this study, the residual cohesion was assumed to be 0.15MPa (c_r=c_p×10%=0.15MPa, φ_r=φ_p=20°), corresponding to a 90% reduction relative to the peak cohesion, as shown in Figure 21(a). The result indicates that the plastic region radius is 4.49m, which is 11.225 times the borehole radius, and this value is smaller than the field test data. In fact, a 90% reduction in cohesion is extremely rare in coal seams, which also indicates that it is inappropriate to consider only the reduction in cohesion. Fan et al. (2019) also reported that the residual cohesion and residual internal friction angle exert a significant influence on the deformation distribution of coal. Subsequently, the plastic softening behavior of the two parameters is incorporated into next analysis. The calculation parameters were set based on the attenuation ratio reported by Fan et al (2019), as follows: the residual cohesion was assigned a value of 0.30MPa (c_r=c_p×20%=0.30MPa), corresponding to a 80% reduction relative to the peak cohesion, and the residual internal friction angle was set to 12° (φ_r=φ_p×60%=12°), representing a 40% reduction relative to the peak internal friction angle. Thus, the calculated plastic region radius is 5.13m, which is 12.825 times the borehole radius, and this value is very close to the field measured value of 5m, as shown Figure 21(a).

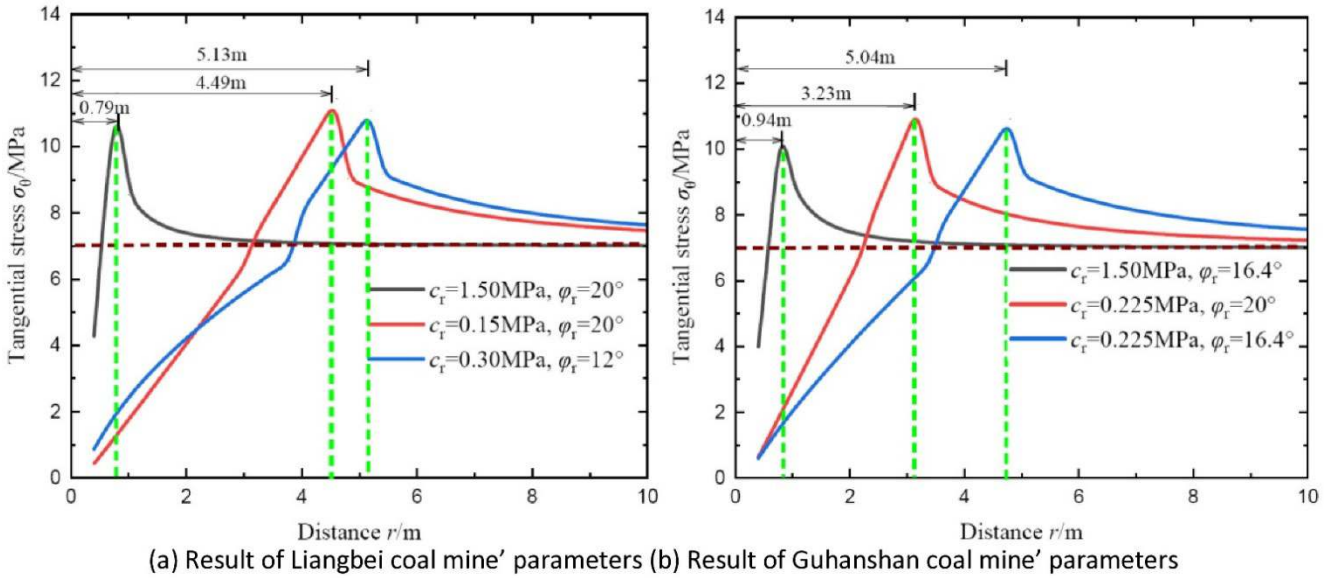


Figure 21 Stress distribution zones surrounding the borehole

To have a better comparison, the plastic softening parameters were collected from the 2_1 coal seams at the Guhanshan coal mine in Henan Province, China by Tu et al. (2019). Guhanshan coal mine and Liangbei coal mine are both located in the same province and exhibit strong geological similarities. From the analysis of test data, the residual cohesion was reduced by 85.08% compared with the peak cohesion, while the residual internal friction angle was reduced by 18.11% compared with the peak internal friction angle. Then the calculated parameters are set as follows: the residual cohesion is assigned a value of 0.225MPa (c_r=c_p×14.92%=0.224MPa), and the residual internal friction angle is set to 16.4° (φ_r=φ_p×82.11%=16.4°). When both of these two plastic softening parameters are considered into the calculation, the plastic region radius is 5.04m; when only the residual cohesion is considered, the plastic region radius is 3.23m. However, when only the residual friction angle is considered, the plastic region radius is only 0.94m, which is much smaller than the field test results, and the result as shown in Figure 21(b).

Figure 22 presents a comparison between numerical simulations considering plastic softening and field tests. It can be seen that the plastic region is circular in both cases, and the numerical results are slightly larger than the measured values. The relative error between the two results is 11.82%, which proves that this method is practically applicable. Additionally, a lateral pressure coefficient λ=1.0 represents a special case of the proposed theoretical model. Therefore, combined with the above comparisons, the rationality of the proposed method in this study is also verified.

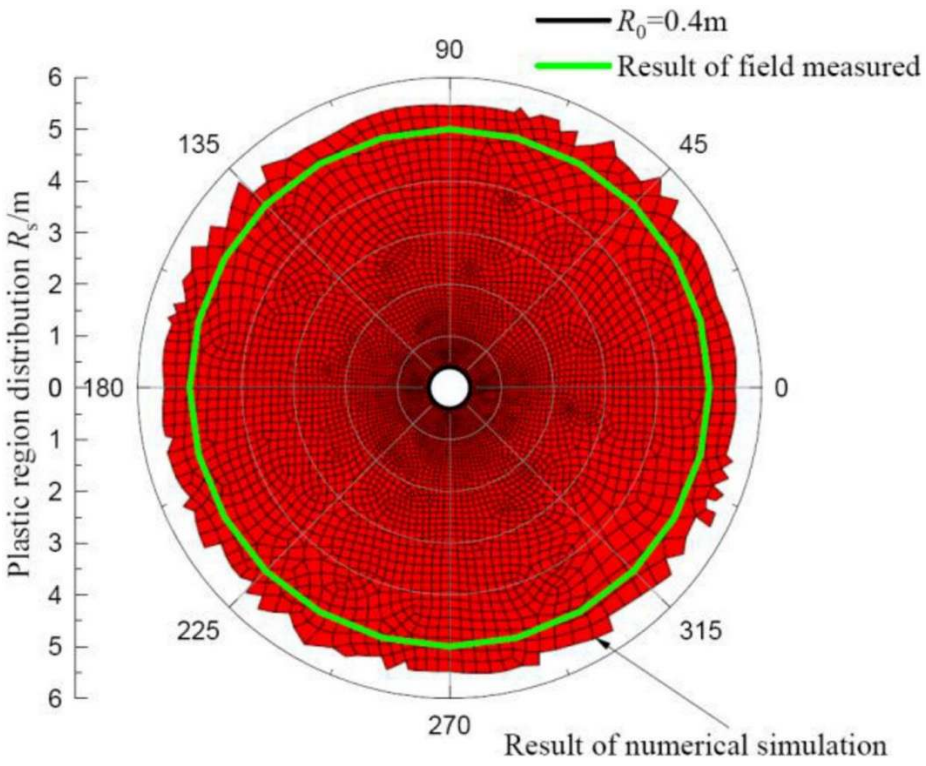


Figure 22 Comparison between numerical results and field tests

8 Conclusion

The objective of this study is to clarify the effects of plastic softening of strength parameters on the stress and deformation characteristics of the coal around the borehole. As a result, the variation law of strength parameters after the stress peak is revealed through a series of experimental data, and a theoretical analysis model for the coal surrounding borehole that incorporates different deformation characteristic is established. The accuracy of the proposed theoretical model is verified by the numerical simulation and field test data. The key findings of this study are summarized as follows:

1. Based on the collection of previous test data from 20 groups of coal samples, it can be concluded that the essence of the plastic softening characteristics exhibited by coal strength parameters is that not only does cohesion decrease, but the internal friction angle also changes. The change rule of the internal friction angle after the stress peak is not fixed, which manifests as an increase, a decrease, or no change, depending on factors such as coal categories. Hence, it is unscientific to mechanically judge whether the residual internal friction angle is useful or should be ignored. Its applicability in engineering practice must be determined based on triaxial test data.

2. A theoretical analysis model for the stress and deformation distribution surrounding the borehole, which includes three characteristic regions, is deduced. Meanwhile, a two-dimensional numerical model is also established to verify the analytical results of the theoretical model. The results show that the plastic region radius will gradually increase as the residual strength parameters decrease, and the lateral pressure coefficient is the primary factor determining the shape of the plastic region. When comparing the simulated tangential stress and plastic region size, the relative error is limited to 12%, which verifies the accuracy of the theoretical solution.

3. The field test data show that the plastic deformation zone has a radius 12.5 times that of the borehole. When only the residual cohesion is considered, the plastic region radius is smaller than that from the field test data. In view of the softening degree of the coal strength parameters, and considering that the calculated results of the residual cohesion and residual internal friction angle are closer to field reality, it is demonstrated that the residual friction angle constitutes another critical factor contributing to the significant discrepancy between calculated results and field test data.

Acknowledgments

This research was funded by Project of Spark Program for Earthquake Sciences, China Earthquake Administration (XH26050A), Langfang Science and Technology Research and Development Plan Project (2025011058) and Hebei Natural Science Foundation (No. E2021512002).

Author's Contribuitions: Conceptualization, investigation, methodology, YL Lu; original draft, XR Chen and YL Lu.; writing and editing the draft, XR Chen and YL Lu.; data processing, XR Chen.

Data availability statement: Research data is only available upon request.

Editor: Pablo Andrés Muñoz Rojas.

References

Ajeet Y, Bhaskara B, Gauri SPS, Sanjay KS (2024). Numerical modelling of post-failure behaviors of coal specimens, Journal of Rock Mechanics and Geotechnical Engineering, 16(2):514-531.

Anuj A, Nishant R (2023). Mechanical response of a circular tunnel under anisotropic stress conditions using the Hoek–Brown strain-softening model, International Journal of Geomechanics, 23(11):1-18.

Brown ET, Bray JW, Ladanyi B, Hoek E (1983). Ground response curves for rock tunnels. Journal of Geotechnical Engineering, 109(1):15-39.

Cui JQ, Hou YB, Xie SR, Chen DD, Yan XX, Ren YX (2023). Analysis and verification of stress and plastic zone in surrounding rocks of hydraulic flushing borehole based on strain-softening. Geomechanics and Geophysics for Geo-Energy and Geo-Resources, 9(1):64.

Deng Q, Tang H, Wang DY, Qin YQ, Wu ZJ (2018). Bench-shape slope stability analysis based on strain softening model. Rock and Soil Mechanics, 39(11):4109-4116.

Fan H, Wang LG, Liu WR (2020). An analytical solution for stresses and deformations of tunnels in a non-uniform stress field based on strain-softening model and Mogi-Coulomb criterion, Latin American Journal of Solids and Structures, 17(1): e246.

Gao FQ, Kang HP (2017). Experimental study on the residual strength of coal under low confinement, Rock Mechanics and Rock Engineering, 50(2):285-296.

Geng JS, Cao LW, Zhong CY, Wang H, Chen BQ (2023). Investigation of dynamic response of drilling parameters and deformation characteristics of coal around borehole during multi-stage reaming in tectonic coal. International Journal of Rock Mechanics and Mining Sciences, 170:105540.

González-C, Varas F, Bastante FG, Alejano LR (2013). Ground reaction curves for circular excavations in non-homogeneous, axisymmetric strain-softening rock masses. Journal of Rock Mechanics and Geotechnical Engineering, 5(6):431-442.

Han JX, Li SC, Li SC, Yang WM, Wang L (2013). Study of post-peak stress-strain relationship of rock material based on evolution of strength parameters, Rock and Soil Mechanics, 34(2):342-346.

Han Y, Zhao QF, Zhang FY (2018). Comparative research on mechanical properties of coal specimens and coal mass based on Hoek-Brown criterion, Journal of Henan Polytechnic University (Nature Science), 37(1):23-30.

He SQ, Ou SN, Lu Y, Jin LZ, Chen T, Ma YR (2022). Failure mechanism of methane drainage borehole in soft coal seams: Insights from simulation, theoretical analysis and in-borehole imaging, Process Safety and Environmental Protection, 168: 410-421.

Jin JC, She CX, Shang PY (2021). Evolution models of the strength parameters and shear dilation angle of rocks considering the plastic internal variable defined by a confining pressure function, Bulletin of Engineering Geology and the Environment, 80:2925-2953.

Jing W, Xue WP, Yao ZS (2018). Variation of the friction angle and cohesion of the plastic softening zone rock in roadway surrounding rock. Journal of China Coal Society, 43(8):2203-2210.

Joseph TG. Estimation of the post-failure stiffness of rock (2000), Alberta, Canada: University of Alberta.

Li GS, Li XQ, Cai B (2009). Experimental study of outburst coal samples and non outburst coal samples on triaxial compression, Chongqing Academic Annual Meeting 2009 of Chongqing Mechanics Society.

Li GY, Zhang BY, Yu YZ (2013). Soil mechanics second edition; Beijing: Tsinghua University Press.

Li WT, Li SC, Feng XD, Li SC, Yuan C (2011a). Study of post-peak strain softening mechanical properties of rock based on Mohr-Coulomb criterion, Chinese Journal of Rock Mechanics and Engineering, 30(7):1460-1466.

Li YS, Yang YJ, Yang SQ, Ma ZG (2011). Deformation and acoustic emission behaviors of coal under triaxial compression and pore water pressure, Journal of University of Science and Technology Beijing, 33(6):658-663.

Liu XB (2018). Strength properties of coal and its influence factors, Chongqing: Chongqing University.

Li Y, Cao SG, Nicholas F, Liu YB (2015). Elasto-plastic analysis of a circular borehole in elastic-strain softening coal seams, International Journal of Rock Mechanics & Mining Sciences, 80:316-324.

Liu YF, Li S, Tang DZ, Xu H, Tao S, Hu X, Zhu XG, Ma L (2019). Mechanical behavior of low-rank bituminous coal under compression: An experimental and numerical study, Journal of Natural Gas Science and Engineering, 66:77-85.

Lu XG, Ji HG, Yu XM, Jiang H, Gao Y, Wu HY (2022). Mechanical characteristics and energy dissipation evolution of coal under triaxial unloading, Journal Harbin Institute of Technology, 54(2):90-98.

Pan JL, Gao ZN, Ren FH (2018). Effect of strength criteria on surrounding rock of circular roadway considering strain softening and dilatancy, Journal of China Coal Society, 43(12):3293-3301.

Simanjuntak TDYF, Marence M, Mynett AE, Schleiss AJ (2014). Pressure tunnels in non-uniform in situ stress conditions, Tunnelling and Underground Space Technology, 42:227-236.

Su CD, Zhai XX, Li YM, Li SM, Liu ZY (2006). Study of deformation and strength of coal samples in triaxial compression, Chinese Journal of Rock Mechanics and Engineering, 25(Supp.1):2963-2968.

Tong GQ, She CX, Zhang HL, Wang JY, Mei XL (2024). A new practical model for the evolution of post-peak strength parameters of rocks, Engineering Journal of Wuhan University, 57(1):45-54.

Tu QY, Cheng YP, Ren T, Wang ZY, Lin J, Lei Y (2019). Role of tectonic coal and gas outburst behavior during coal mining, Rock Mechanics and Rock Engineering, 52(11):4619-4635.

Wang EY, Wang H, Liu XF, Shen RX, Zhang CL (2020). Spatio temporal evolution of geostress and gas field around hydraulic punching borehole in coal seam, Coal Science and Technology, 48(1):39-45.

Wang JY (2010). Experiment research on the effect confining pressure on physical properties of coal, Safety in Coal Mines, 41(12):14-16.

Xu C, Qin LL, Wang K, Wu SM, Zhang R, Guo HJ, Shu LY (2023). Deformation and failure characteristics of gas drainage drilling-reaming coal mass in non-uniform stress field, Journal of China Coal Society, 48(4):1538-1550.

Yang SP, Liu PZ, Lu WY (2023). Study on triaxial compression tests on briquette coal specimens with different binder contents, Journal of Mining and Strata Control Engineering, 5(2):023026.

Yang SQ, Hu B, Xu P (2019). Study on the damage-softening constitutive model of rock and experimental verification. Acta Mechanica Sinica, 35(4):786-798.

Yang YJ, Song Y, Chen SJ, Li TC (2006a). Experimental study on strength discreteness and triaxial compression of coal, Rock and Soil Mechanics, 27(10):1763-1766.

Yang YJ, Song Y, Chen SJ (2006b). Test study of coal's strength and deformation characteristics under triaxial compression, Journal of China Coal Society, 31(2):150-153.

Yang Z, Guo AW (2023). Study of mechanical properties and energy evolution law of coal under cyclic load, China Coal, 49(3):42-47.

Zhang F, Sheng Q, Zhu ZQ, Zhang YH (2008). Study on post-peak mechanical behavior and strain-softening model of three gorges granite, Chinese Journal of Rock Mechanics and Engineering, (Supp.1): 2651-2655.

Zhang J, Wen GH, Sun ZB, Zhu JP, Dong RZ, Li XH, Shi Z, Meng QB, Sun W, Chen YL (2022). Experimental study on deformation and evolution characteristics of coal samples under high stress, Journal of Henan Polytechnic University (Nature Science), 41(6):1-7.

Zhang L, Li XC, Ren T (2020). A theoretical and experimental study of stress–strain, creep and failure mechanisms of intact coal, Rock Mechanics and Rock Engineering, 53(12):5641-5658.

Zhang XF, Lu YL, Yin HC, Guo X, Wang H, Chen Y (2025). Mechanical characteristics analysis of coal around borehole based on three-stage constitutive model and its numerical validation, Scientific Reports, 15:15792.

Zhang XF, Lu YL, Li GY, Yin HC, Guo X, Chen Y, Wang H (2026). Study on cross-sectional selection method and mechanical properties of a radial stressmeter with multipetal structure, Advances in Civil Engineering, 2026:4953390.

Zhang Y, Ren JH, Chen ZQ (2015). Different lithologies coal and rock under the triaxial compression strength and deformation characteristics, Journal of Xi'an University of Science and Technology, 35(6):708-714.

Zhang YJ, Zhang DP, Feng GR, Zhang S, Chen YM, Zhang XF, Wang Q, Cui DL (2024). Characteristics of penetration strength and fracture features under nonuniform stress field around borehole surrounding rock. ACS Omega. 9(24):26168-26182.

Zheng YR, Zhu HH, Fang ZC, Liu HH (2012). The stability analysis and design theory of surrounding rock of underground engineering; Beijing: China Communications Press.

Zhu YJ, Li P, Wang P, Ren H, Tao W, Mei CC, Wang XZ (2023). Experimental study on radial gradient damage characteristics of surrounding rock in deep high stress coal roadway, Chinese Journal of Rock Mechanics and Engineering, 42(11):2643-2654.